Spring 2014

Effect of stress concentrations on fatigue of composite and metallic structures

Ross Henry Falen

Department:

EFFECT OF STRESS CONCENTRATIONS ON FATIGUE OF COMPOSITE AND METALLIC STRUCTURES

by

ROSS HENRY FALEN

A THESIS

Presented to the Faculty of the Graduate School of the

MISSOURI UNIVERSITY OF SCIENCE AND TECHNOLOGY

In Partial Fulfillment of the Requirements for the Degree

MASTER OF SCIENCE IN MECHANCIAL ENGINEERING

2014

Approved by

Dr. Lokeswarappa R. Dharani, Advisor

Dr. K. Chandrashekhara

Dr. Jeffery Thomas

ABSTRACT

The complex shapes of hydrokinetic turbine blades can include part features such as a fillet, step, or hole. Situations can arise where two part features, such as a hole and a fillet, may be in close proximity which can introduce stress concentrations within the blade structure, adversely affecting the structure's life. Because the interaction between the part features isn't well known, fatigue data is needed to determine the proper analysis.

In this thesis, two separate topics are discussed and investigated. The first topic deals with stress concentrations in hydrokinetic turbine blades. Several blade designs were tested and improved upon to increase blade strength and stiffness, insuring that the blade failed due to material limits. These test results were then compared with those from a finite element (FE) model replicating the physical test. Fatigue performance was also tested with an accompanying unloading stiffness test to determine the loss of stiffness within the blade. There was a good agreement between the failure loads determined from the tests and the FE model. The associated strain values had major discrepancies but followed similar trends, suggesting a strain gauge calibration error. For the associated blade geometry, the results indicate that fatigue does not play a significant role in the degradation of the blade life cycle.

The second topic deals with a unique interaction between a hole and a fillet in a flat aluminum alloy specimen. The interaction between the two part features was analyzed to determine the stress concentration modification factor. For the associated geometry, the stress concentration modification factors increased as the distance between the hole and fillet decreased. For fatigue analysis of a hole interacting with a fillet, a conservative modification factor of 1.15 is recommended.

ACKNOWLEDGMENT

I would like to express my appreciation to my advisor Dr. Lokesh R. Dharani for providing me with a project to expand my research and technical skills. I also appreciated your support and guidance during my research and studies here at Missouri S&T. I would like to thank Dr. K. Chandrashekhara and Dr. Jeff Thomas for providing me with the facilities and equipment to conduct my research.

I express my gratitude to Randall Lewis of the Toomey Hall machine shop and Ron Hass of the Material Research Center machine shop. Without their machining and fabrication experience, I could not have been able to fabricate the fixtures and test stand needed to test my material specimens.

Greg Taylor, James Nicholas, Abdulaziz Abutunis, Zhen Huo, and David Whitley deserve credit for the numerous times that they offered advice and personally helped me with the experimental side of the project.

To my parents, David and Susie Falen, and my friends, I appreciate your ongoing support. Without your confidence and encouragement, I would not be the person I am today.

TABLE OF CONTENTS

Page

LIST OF ILLUSTRATIONS

LIST OF TABLES

1. INTRODUCTION

The world currently relies on fossil fuels for energy production, amounting to 85% of the total energy production. Fossil fuels are nonrenewable and include fuels such as coal, petroleum, and natural gases. Though these sources are adequate in producing energy, they are a finite resource, environmentally damaging, and becoming more and more expensive. To combat these issues, renewable energy resources are being produced.

Most renewable energy today comes directly or indirectly from the sun, called solar energy. Solar energy uses solar radiation and can be used to produce heat, lighting, and generate electricity. Solar radiation is captured and converted to electrical energy through the use of solar panels. Along with sunlight, rain and snow help plants grow. Plants capture the sun's energy through the process of photosynthesis. The organic matter contained in the plants, biomass, can then be burnt, releasing the energy contained. Energy released in this way is referred to bio-energy. Bio-energy can be used to produce electricity, fuels for transportation, or chemicals. Hydrogen is the most abundant element on earth and can be found in most organic compounds. Hydrogen does not occur naturally, as it is always combined with other elements. If separated, hydrogen can be burned directly as a fuel or converted into electricity.

The sun’s heat also drives Earth's winds. Wind energy is essentially solar energy since the sun produces an uneven heating of the atmosphere, causing a breeze to blow. This energy, referred to as wind energy, is captured with wind turbines. As wind blows past the turbine blades, a low pressure system occurs on the trailing edge of the blade. This pressure difference causes the blades to rotate around a rotor. This rotor rotates

around an axis, spinning a generator used to create electricity. Water energy comes from a number of sources. These sources include tides, winds, and temperature differences. Tides are produced from the sun and the moon's gravitational pull upon the earth. Currently, water power is largely the cheapest of all the renewable energies for producing electricity, but hydroelectric dams have caused many environmental controversies due to their ecological disruptions. Because of this, ocean energy is taking advantage of the movement of water in tides and waves.

The total long term potential of tidal and wave energy is equal to the long term potential of onshore wind energy [1]. This is because of the abundance of natural water sources with untapped potential. Therefore, the interest in the development of hydrokinetic systems is increasing. Hydrokinetic systems generate electricity by utilizing the kinetic energy contained in river streams, tidal currents, or other man-made waterways [2]. This kinetic energy is produced from the initial downward force of the water and combining waterway.

This unique and promising way to produce energy is an emerging class of renewable energy technology. This is because it offers multiple benefits such as less environmental and ecological impact, lower initial cost, and lower maintenance, as compared to conventional dam based hydropower [3]. Hydrokinetic turbine systems don't restrict the flow of a natural river source and are generally much smaller than conventional dams. Still, hydrokinetic energy technologies are lagging far behind the wind renewable energy industry.

The horizontal axis turbine is the most commonly used system in wind energy; whereas many different techniques are still being developed for hydrokinetic energy.

Much of the knowledge required to develop reliable and profitable marine energy systems is available in the wind energy sector [4]. This is because the two types of systems share similar designs, such as a vertical axis system. These systems experience similar loading cases. This is because the two setups generate energy in the same way but are produced through different mediums, air or water. The random nature of ocean current means the blade will experience a significant number of fatigue cycles over its expected lifespan [5]. Both will experience fluctuations in medium flow producing repeated applied loads, causing the blades to be fatigued.

The fatigue process begins with microscopic and macroscopic discontinuities within the structure. These discontinuities cause an increase in the intensity of the local stress in the stress field, referred to as a stress concentration [6]. The intensity of the stress concentration is measured by the stress concentration factor, SCF, and is typically denoted by the symbol K_t. The SCF in its simplest form is defined as the ratio of the highest local stress to a reference stress. The most common stress concentration factor describes a hole located in the center of an infinite plate, loaded in tension, as seen in Figure 1.1. The stress distribution due to the hole is shown. For this situation, as D/W goes to zero, $K_t = 3$.

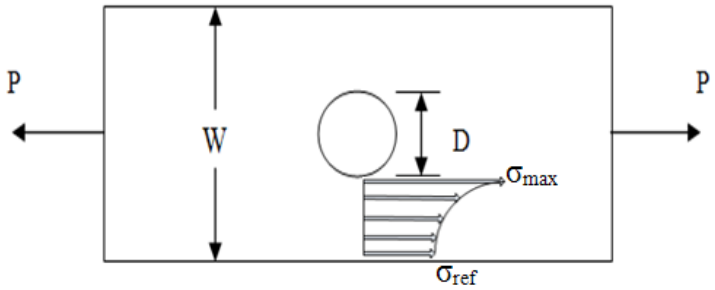

Figure 1.1 - Infinite Plate with Centralized Hole Loaded in Tension [7]

There are many different sources that provide K_t charts for parts containing various geometries, loading conditions, and features. SCF's are not universal, so engineers must reference these charts to ensure the SCF accurately represents their specific analysis of metallic structures. The preferred handbook for SCF values is Peterson's Stress Concentration Factors [8, 9]

Stress concentration factors are an important aspect of any fatigue analysis. Cracks generally nucleate in an area where stress is at its maximum, thus, they are most likely to nucleate at a stress concentration. Because of this, proper stress concentration factors must be used to calculate the maximum stresses the structure will see and are essential in accurately predicting the fatigue life. For fatigue analysis, the net stress concentration factor, K_{nt}, must be calculated to accurately determine the maximum stress the structure experiences.

The net stress concentration factor accounts for the net cross-sectional area at the location of interest, whereas the gross stress concentration factor, K_{tg}, accounts for the overall cross-sectional area at the location of interest. Consider a flat plat with a centrally located hole, loaded in tension, with a thickness, h, Figure 1.2. The peak stress occurs at the critical points, C. Using the reference stress factor for both K_{tn} and K_{tg}, the difference between the two factors can be determined, as shown in Equations 1 through 3.

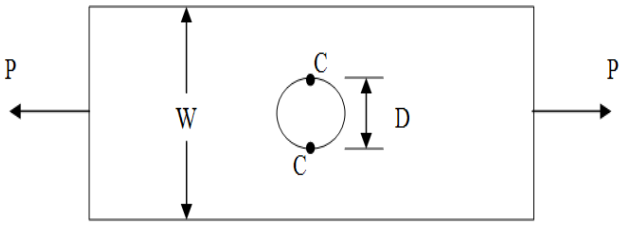

Figure 1.2 - Plate with Centralized Hole Loaded in Tension [7]

$$K_{tn} = \frac{\sigma_{\max}}{\sigma_{\text{ref,net}}} = \frac{\sigma_{\max}(W-D)h}{P} \quad (1)$$

$$K_{tg} = \frac{\sigma_{\max}}{\sigma_{\text{ref,gross}}} = \frac{\sigma_{\max}Wh}{P} \quad (2)$$

$$K_{tn} = K_{tg}\frac{(W-D)}{W} \quad (3)$$

The preceding equations illustrate that the net stress concentration factor accounts for discontinuity in the center of the plate, whereas the gross stress concentration factor only accounts for the width of the plate.

Some geometry may involve the interaction of two or more features. For example, consider the following, a hole in a radius as shown in Figure 1.3. Graham, Raines Swift and Gill [10] and Graham [11] have developed SCF for the situation shown in Figure 1.3. Stress concentration factors for these kind of situations are developed by means of experimental testing and are dependent on many variables such as hole diameter, plate width, and amount of interaction between the center of the hole and the root radius. Holes drilled at or near a radius occur frequently in aero-structures, and during manufacture situations can arise where the hole is mislocated. This can create a situation where the hole interferes with the radius. It is assumed that repair measures are not possible. Because of this, K_t modification factors are used to properly account for the effects of the hole interacting with a part feature. A typical configuration used to analyze the SCF in this situation is displayed in Figure 1.4.

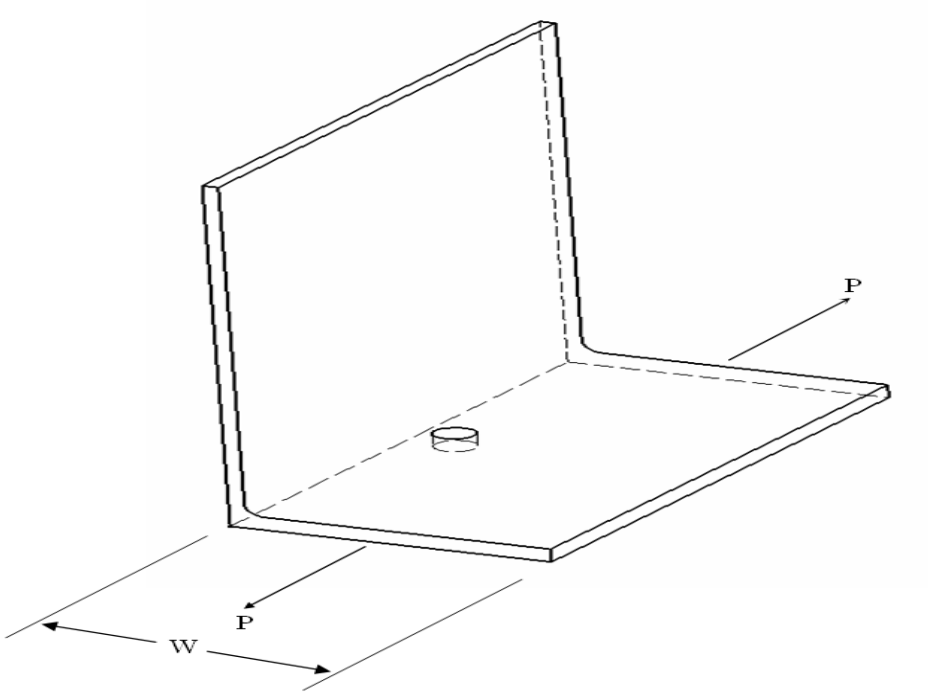

Figure 1.3 - Hole Located in a Radius with Axial Tension Applied [7]

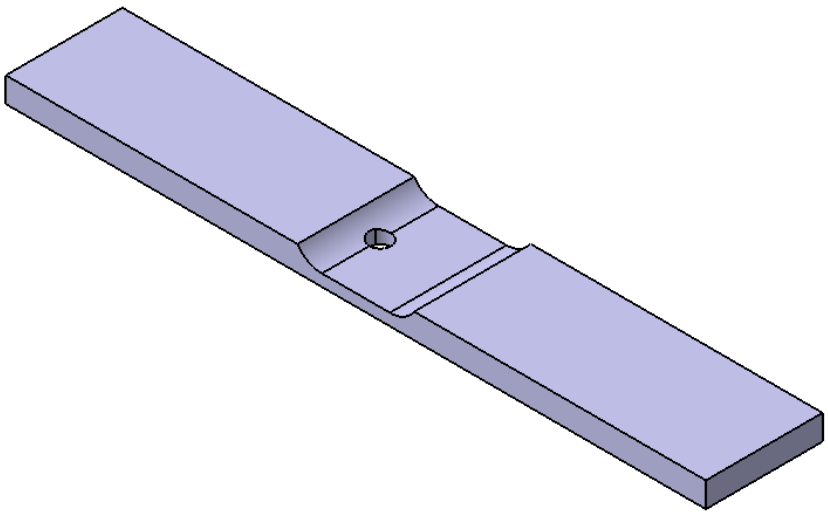

Figure 1.4 - Open Hole in Radius Test Specimen [7]

To address the two important problems highlighted above, this thesis will be broken up into two distinct parts. The first part will address details of composite blade performance and life. The blade design and laminate will be discussed. The experimental methods will be thoroughly described including the introduction of stress and fatigue. Lastly, a collection of data plots will be presented to illustrate the effects of the above parameters. The second part will address the issues of interacting part features and their corresponding stress modification factors. To find the stress concentration modification factors, K_{tf}, an in-depth study through testing of the SCF interaction between the hole and radius, based off positioning, is conducted.

2. REVIEW OF LITERATURE

As with any structure, the design is driven by the forces that cause loads on the structure. Wind and hydrokinetic turbines experience various types of loads throughout their work life. The forces that cause loads on turbine blades are aerodynamic, inertia, and gravity forces. Aerodynamic forces, such as lift and drag, are generated by an object with an angle of attack moving through a fluid. A fluid can be any medium, such as air or water. These forces turn into normal and tangential loads which produce moments, thrust, torque and power on the turbine rotor. Inertial forces are forces generated by the rotation of the blades around the hub axis. This happens when the turbine blades are accelerated or decelerated. Gravity forces are caused by the weight of the blades. Considering the variation of these loads at any given time, they can be grouped together to produce steady static loads. Generally, the loads experienced by turbine blades are considered as dynamic or cyclic loads.

Basic cyclic tests are performed at a constant stress level, generally a percentage of the material's ultimate strength. Because of this, static loading cases need to be performed to find the material properties of the blade. To find the ultimate strength of a material, a constant displacement rate must be applied to the material. The maximum force applied to the material at failure will be used to determine the ultimate strength. Ultimate strength should be measured at the normal quasi-static loading rate of 1-10 mm/min [12].

During its lifetime, a wind turbine is subjected to a large number of dynamic loads produced by the rotation of the blades as well as the turbulent nature of wind on the

blades [13]. This means that the loads experienced by the turbine blades will vary with time. The random nature of water current means the blade will experience a significant number of fatigue cycles over its expected lifespan [14]. These random fluctuations in water current are due to various environmental effects. These effects can be changes in temperature, wind speed, water salinity, and tides. Because of these load fluctuations, fatigue is a major problem with hydrokinetic turbine blades. Fatigue is a phenomenon that causes a gradual reduction in the operating capacity of the material when subjected to cyclic loading [13]. The simplest type of cyclic loading is constant amplitude fatigue. This means that the applied stress alternates between two stress values, S_{max} and S_{min}. These are the maximum and minimum stress achieved during cyclic loading. The ratio of the minimum stress to the maximum stress is referred to as the stress ratio, R, and is used to characterize the type of fatigue loading. The two most common R conditions for obtaining fatigue properties are $R = -1$ and $R = 0$. $R = -1$ is considered the "fully reversed" condition, where S_{max} and S_{min} are equal and opposite. $R = 0$ is considered "pulsating tension", where the stress cycles between zero and S_{max}. These two conditions are shown in Figure 2.1.

Fluctuations in current alter the loading placed on the blades, producing alternating stresses. The most dominant sources of alternating stresses are due to the randomness of ocean current and velocity shear [14]. The combination of these loadings will result in alternating flap wise bending. Alternating flap-wise bending produces more than 90% of the fatigue damage in both wind turbine [5] and water turbine blades. Thus, flap-wise bending will be the focus of the cyclic test in this study. Both maximum energy and maximum damage are accumulated if the wind turbine is operated (on) at all times

[15]. Damage accumulated while the turbine is parked and during start-stop cycles is included; data collected support the assumption that these events have negligible effects on blade fatigue life [15]. Thus, constant stress fluctuations or a constant stress ratio can accuracy model fatigue life in turbine blades. For blades longer than 10 m, the bending stresses become large with respect to fatigue failure, due to the significant dependence of hydrodynamic loading on the blade length [16]. Thus, for the blades smaller than 10 m in length, fatigue failure will be the dominant factor in blade failure. Single point hydraulic loading has the benefit of being a simple and robust way to fatigue load a blade but cannot match the desired load distribution as well as other loading methods [17].

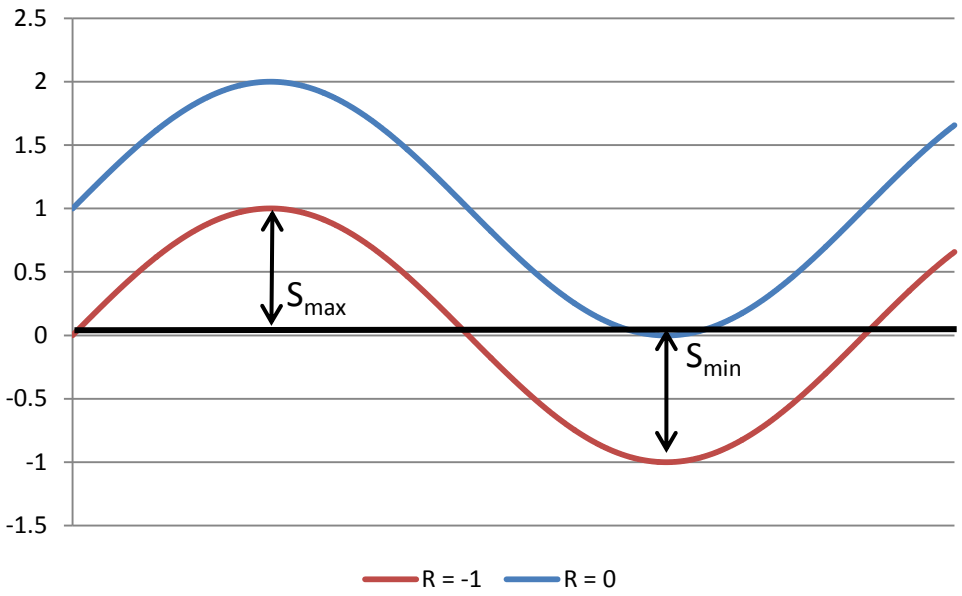

Figure 2.1 – Common Stress Ratio Cyclic Loading Profile

Generally, water sources flow in one direction. Since flow doesn't change direction, the loading on the blade will remain in the same direction. Because of this,

stress cycles in turbine blades generally have a non-zero mean value [13]. This means the magnitude of the load will change but the loading direction will remain the same, meaning the blade will experience a positive stress ratio, *R*.

R-ratio of 0.1 on the high pressure surface of the blade is desired as it simulates operational conditions [17]. Figure 2.2 displays the effect it has on the specimen for an *R*-value of 0.1. Since the load amplitude is kept constant, this type of fatigue is considered stress control mode. This control mode is preferred for the derivation of an S-N Curve. Here *S* is the applied nominal stress, usually taken as the alternating stress, S_a, and *N* is the number of cycles to failure, where failure is defined as fracture [18].

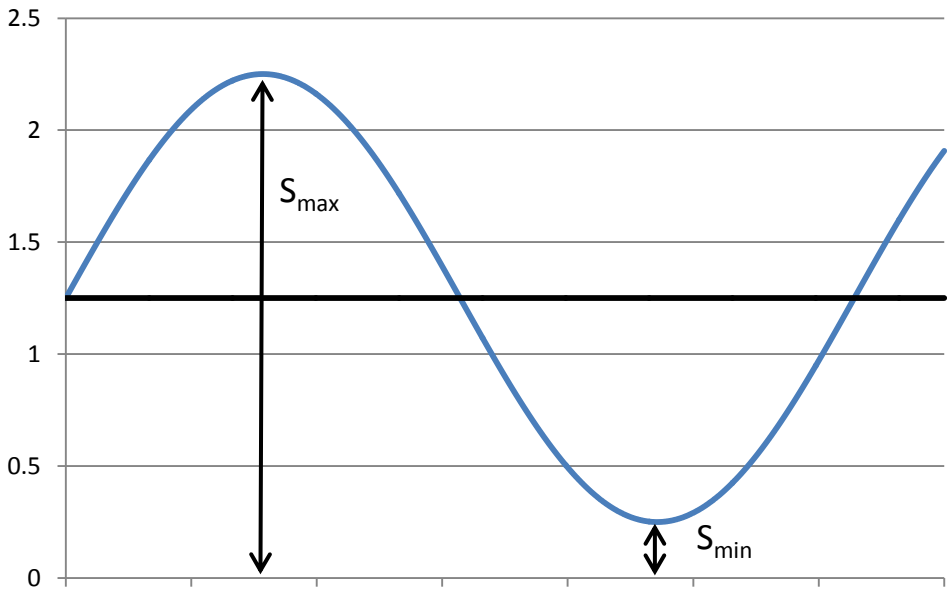

Figure 2.2 – Stress Ratio, *R* = 0.1, Cyclic Loading Profile

Fatigue life of composite material is considerably affected by testing frequency. The dependence is due to heating of the material at higher frequencies and creep fatigue

at lower frequencies [12]. Because of this, composites cannot be tested at the same frequencies as metal fatigue. Thus a lower testing frequency is used for fatigue, 10 Hz. Cyclic tests on composites should be performed at a rate that matches the quasi-static loading rate of the static test.

Fatigue damage is distributed equally throughout the stressed regions, reducing the composite stiffness. Because of this, the strength of the composite is not immediately reduced [12]. An unloading stiffness test is performed periodically throughout the fatigue test. Unloading stiffness finds the ratio of the force to displacement. If the ratio decreases, meaning less force is required to move the test specimen the same displacement, this signals that the specimen stiffness has decreased. Thus the unloading stiffness test finds the rate at which specimen deformation occurs with the increase in cycles.

3. SPECIMEN FABRICATION

To address these two separate issues, two test specimen designs were created. Composite blades were manufactured to test hydrokinetic turbine performance and life. Aluminum coupons were machined to investigate the interaction between a hole and a radius. The first section details the design and fabrication of the composite hydrokinetic turbine blades and the second section deals with the fabrication of the aluminum specimens.

3.1. BLADE DESIGN AND FABRICATION

The blade fabrication went through three separate iterations due to premature failure caused by unforeseen stress concentrations. Each iteration improved upon the previous design by eliminating the known stress concentration and increasing turbine blade performance. The three ensuing blade versions are designated as Design 1.0, Design 1.1, and Design 1.2.

3.1.1. Fabrication of Blade Design 1.0. The specimens used for this experiment were manufactured using an out-of-autoclave process. The blades were constructed using a unidirectional carbon fiber pre-preg, Cycom 5250 [19]. The laminate consisted of a three layer configuration of [0/90/0], with zero along the hydrofoil span. The pre-preg was cut into 15” x 3” sheets. For one blade, this consisted of four sheets with the fibers oriented parallel to the 15” side and two sheets with the fibers oriented parallel to the 3” side. To make the layup, one layer of the pre-preg was placed on a flat surface. A layer

with perpendicular fibers was then placed on top of the previous layer. These layers were then pressed together. A rolling pin was then used to prevent wrinkles in the pre-preg and to ensure a flush fit. The backing from the 90 degree layer was then peeled off. A zero degree layer was then placed onto the 90 degree side. The ply was then pressed and rolled to prevent wrinkles. The backings were then peeled off on the outer edges of the laminate. A sheet of fluorinated ethylene propylene (FEP) was placed on both sides of the laminate. This was used to prevent the laminate from sticking to the mold. The laminate was then taped on one side of the mold to prevent the laminate from moving before a vacuum was applied.

A large aluminum plate was used as the back half of the vacuum bag. Thick, two sided tape was used to make a perimeter for the vacuum seal. A sheet of vacuum bag was cut in excess to complete the sealing process. The molds were then placed on the aluminum. A wool sheet was placed on top of the molds to prevent wrinkles when a vacuum is applied, Figure 3.1. The other side of the tape was peeled, and the FEP was placed on the tape little by little to prevent wrinkles. Wrinkles in the vacuum bag can cause air leaks. Once the vacuum bag was taped completely around the molds, a vacuum was applied to the setup, Figure 3.2. This was done by applying a vacuum with a pump, turning off the pump and checking for a constant pressure. If the pressure changed, a leak detector was used to pinpoint the leak. At the leak location, the bag was either pressed onto the tape to provide a better seal or extra tape was added. Once the vacuum was complete, the laminate was pressed into the mold. This causes the laminate to better fit some of the complex curves present in the mold.

The completed vacuum bag system was then placed in an oven and cooked for a manufacturer-determined cure cycle. The cycle started with a five minute ramp to 100 degrees Fahrenheit, accompanied by a 60 minute soak, then a 45 minute ramp to 250 degrees Fahrenheit, followed by a soak for six hours. Lastly, the composite was cooled down to a temperature of 110 degrees Fahrenheit.

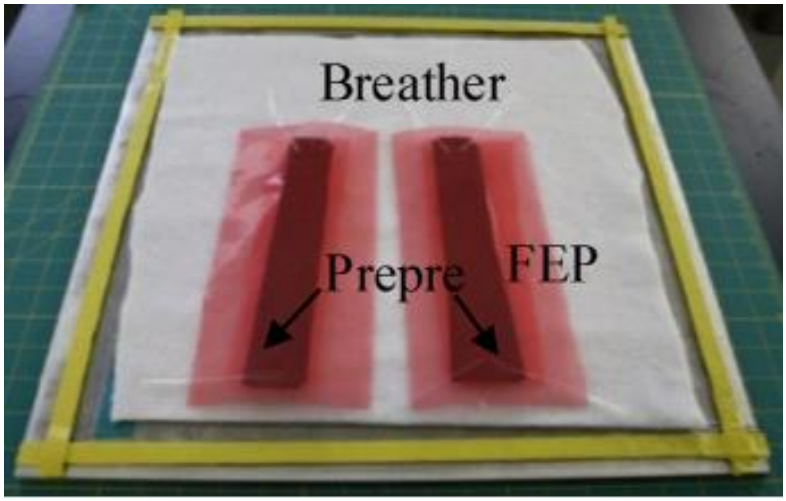

Figure 3.1 – Composite Blade Manufacturing Process Configuration [3]

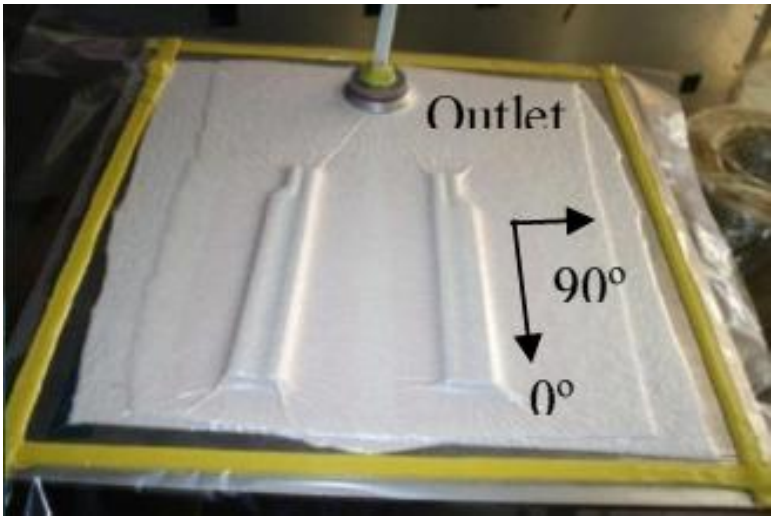

Figure 3.2 – Composite Blade Manufacturing Process Configuration with a Vacuum Applied [3]

Once cured, the two halves were removed from the vacuum bag as shown in Figure 3.3. A two part phenolic epoxy was mixed together to bond the two halves. To mix the epoxy, an even amount of both the resin and the hardener were added to a mixing palette. A round wooden stick was used to mix the two parts together. Once the two parts formed a uniform color throughout, the epoxy was ready to be applied. Each blade half was then placed on the mold with a sheet of FEP. This was used to prevent the epoxy from sticking to the mold. Then a thin layer of epoxy was applied with a uniform thickness along the entire edge of the blade half. This process was then repeated for the other blade half. The two halves were then placed together. Clamps were then placed along the blade length, as required, to apply a constant pressure between the blade halves. The setup was left in this configuration for a minimum of 24 hours, the manufacturer's recommended cure time.

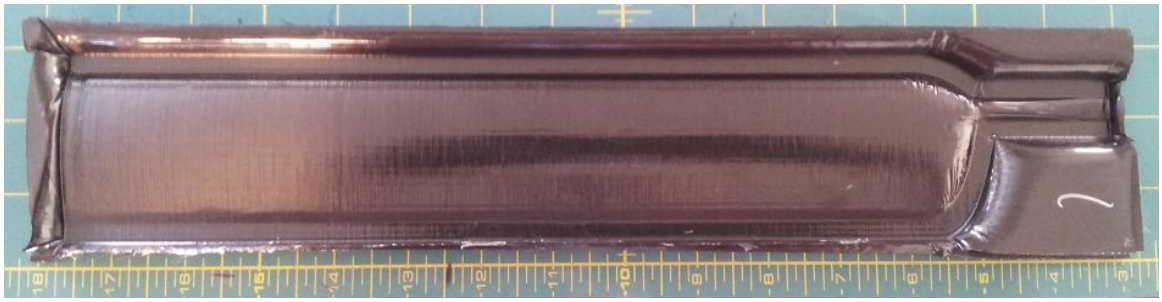

Figure 3.3 – Cured Composite Blade Directly out of Mold

Once the epoxy cured, the excess material had to be removed to create an airfoil shape. A large part of the excess material was removed by using a table saw. To cut the laminate, the blade had to be wet to prevent the composite particles from becoming airborne, as it could be dangerous for your health. The table saw was guided along the

blade shape leaving a small amount of excess material. This material was then removed using wet, low grit sandpaper for easier removal. As the excess material was removed, higher grit sandpaper was used to smooth the edges until the blade formed a uniform shape with rounded edges, as shown in Figure 3.4.

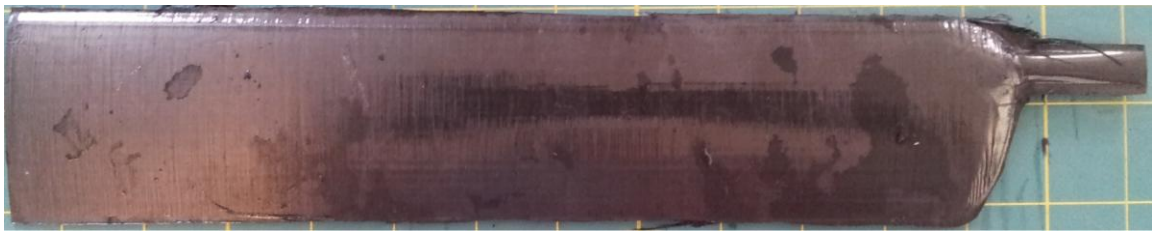

Figure 3.4 – Composite Blade after Excess Material is Removed and Sanded to Shape

3.1.2. Fabrication of Blade Design 1.1. To isolate the blade span and remove the stress concentration present at the root, epoxy tabs were applied at the root and secured to the stand using new aluminum fixtures. To apply the epoxy tabs, a thin layer of lubricant was applied to the aluminum fixture to prevent the epoxy from bonding to the aluminum. The root section was coated in a layer of metal epoxy and placed in the aluminum fixture. The other half of the fixture was then placed on the blade. Pressure was then applied to the fixture. This forced the epoxy to form to the shape of the fixture. More epoxy was force into the fixture to provide a perfect seal. After the epoxy work life, five minutes, pressure ceased and the fixture was separated from the taps. The blade was then set aside for its functional cure cycle, 60 minutes. After this cycle was completed, scissors were used to

remove the excess epoxy from the tabs. The epoxy fixture was then sanded smooth for a tight fit within the aluminum fixture. The finished blade design 1.1 is shown in Figure 3.5.

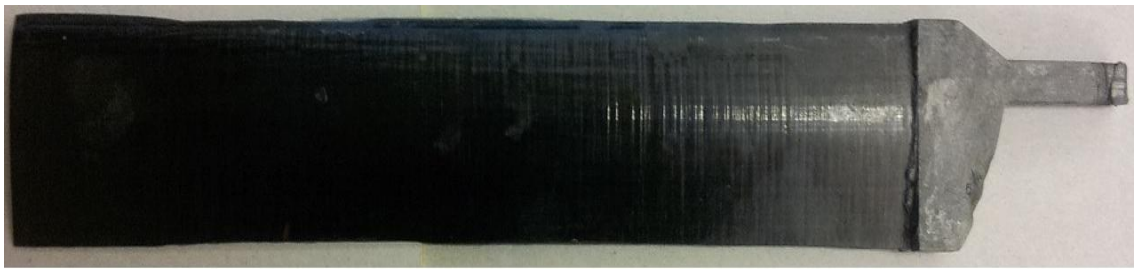

Figure 3.5 – Composite Blade Design 1.1 with Metal Epoxy Tabs Cured to Root and the Area Leading to the Constant Area Cross Section

3.1.3. Fabrication of Blade Design 1.2. To prevent the epoxy from failing, extra layers of pre-preg were wrapped around the blade span and cured. This was done by filling the blade with silica particles to reinforce the blade structure while under vacuum. Three layers of pre-preg were cut to dimension and placed in a stacking sequence of [0/90/0]. The layers were then wrapped around the blade span, taking sufficient care to ensure no air was present between the layers. A layer of FEP was then placed around the pre-preg and secured using adhesive strips. A layer of breather was placed around the blade and then bagged. The structure of this wrapping is shown in Figure 3.1. An outlet tube was then secured to the bag, and the blade was cured at vacuum. The final composite blade design can be seen in Figure 3.6.

Figure 3.6 – Composite Blade Design 1.2 with Metal Epoxy Tabs and Three Extra Layers of Pre-Preg Wrapped and Cured to Blade Span

3.2. FABRICATION OF ALUMINUM OPEN HOLE SPECIMENS

The aluminum specimens were fabricated to the specifications shown in Figure 3.7. These specimens were machined from 2024-T351 plate material. Twenty four specimens were manufactured with hole-to-fillet dimensions including 0.5, 0.3079, 0.2029, 0.2091, and 0.1 inches. Each specimen was permanently engraved with a specimen ID as instructed in the specimen drawing. All holes were drilled in accordance with approved specifications and were reamed and debarred. No holes were drilled in the DW-RKt specimens.

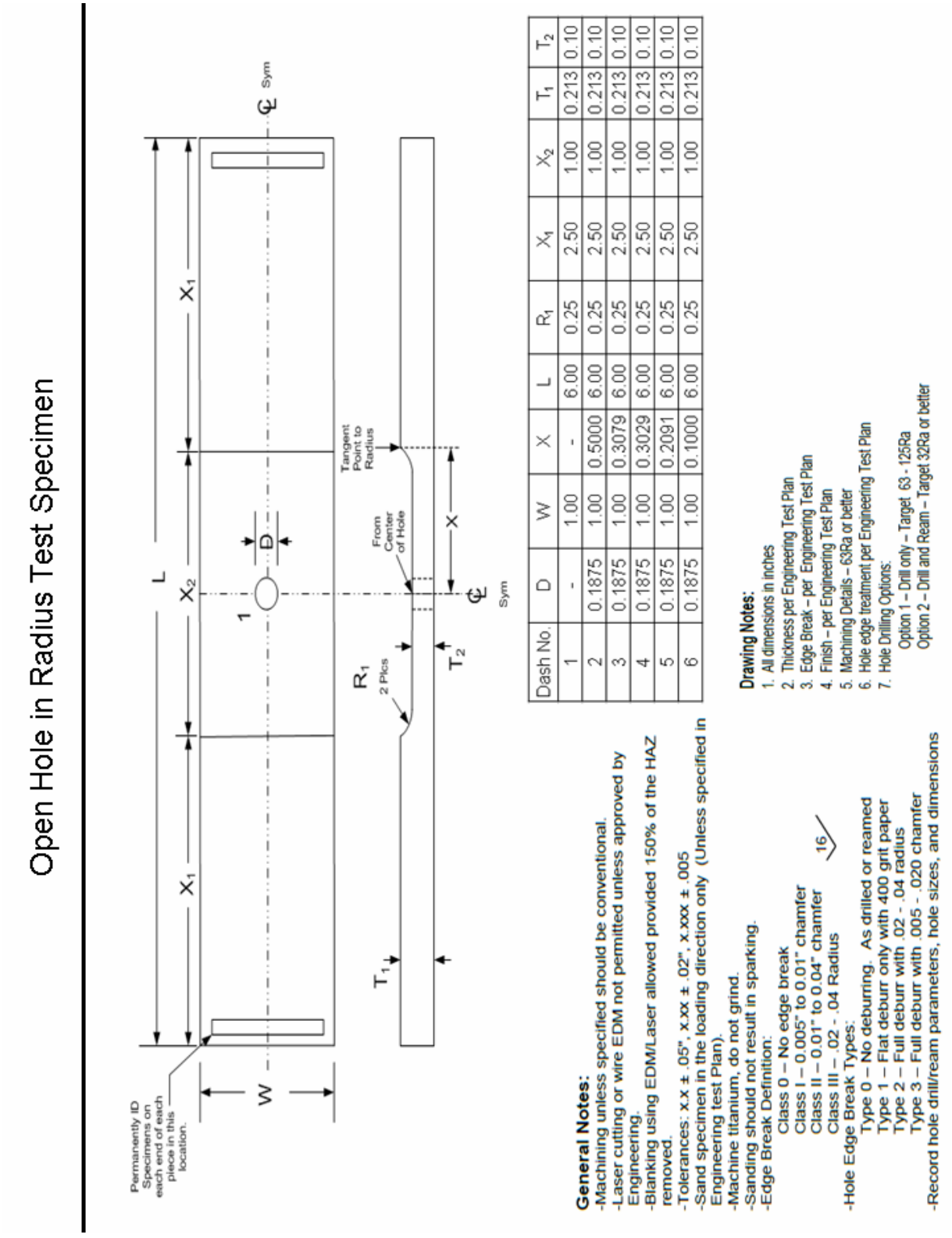

Dash No.	D	W	X	L	R_1	X_1	X_2	T_1	T_2
1	-	1.00	-	6.00	0.25	2.50	1.00	0.213	0.10
2	0.1875	1.00	0.5000	6.00	0.25	2.50	1.00	0.213	0.10
3	0.1875	1.00	0.3079	6.00	0.25	2.50	1.00	0.213	0.10
4	0.1875	1.00	0.3029	6.00	0.25	2.50	1.00	0.213	0.10
5	0.1875	1.00	0.2091	6.00	0.25	2.50	1.00	0.213	0.10
6	0.1875	1.00	0.1000	6.00	0.25	2.50	1.00	0.213	0.10

General Notes:
-Machining unless specified should be conventional.
-Laser cutting or wire EDM not permitted unless approved by Engineering.
-Blanking using EDM/Laser allowed provided 150% of the HAZ removed.
-Tolerances: x.x ± .05", x.xx ± .02", x.xxx ± .005
-Sand specimen in the loading direction only (Unless specified in Engineering test Plan).
-Machine titanium, do not grind.
-Sanding should not result in sparking.
-Edge Break Definition:
Class 0 – No edge break
Class I – 0.005" to 0.01" chamfer
Class II – 0.01" to 0.04" chamfer
Class III – .02 - .04 Radius
-Hole Edge Break Types:
Type 0 – No deburring. As drilled or reamed
Type 1 – Flat deburr only with 400 grit paper
Type 2 – Full deburr with .02 - .04 radius
Type 3 – Full deburr with .005 - .020 chamfer
-Record hole drill/ream parameters, hole sizes, and dimensions

16

Drawing Notes:
1. All dimensions in inches
2. Thickness per Engineering Test Plan
3. Edge Break - per Engineering Test Plan
4. Finish – per Engineering Test Plan
5. Machining Details – 63Ra or better
6. Hole edge treatment per Engineering Test Plan
7. Hole Drilling Options:
Option 1 – Drill only – Target 63 - 125Ra
Option 2 – Drill and Ream – Target 32Ra or better

Figure 3.7 - Open Hole in Radius Test Specimen Dimensions [7]

4. FINITE ELEMENT ANALYSIS

The objective of performing the finite element analysis on the composite blade was to determine the applied force and the strain at specific locations along the blade span at a relative blade deflection. Finite element analysis was only performed for the hydrokinetic turbine blade. Finite element analysis for the open hole specimens is not included because it was performed as a separate project as part of a graduate dissertation [7].

4.1. SIMULATION OF EXPERIMENTAL SETUP

A model was made in Solidworks to exactly model the mold dimensions. This Solidworks model was imported into ABAQUS for analysis. The model was imported as a three dimensional deformable shell, making the model hollow with no surface thickness. The two ends of the blade were removed to replicate the physical blade, as shown in Figure 4.1.

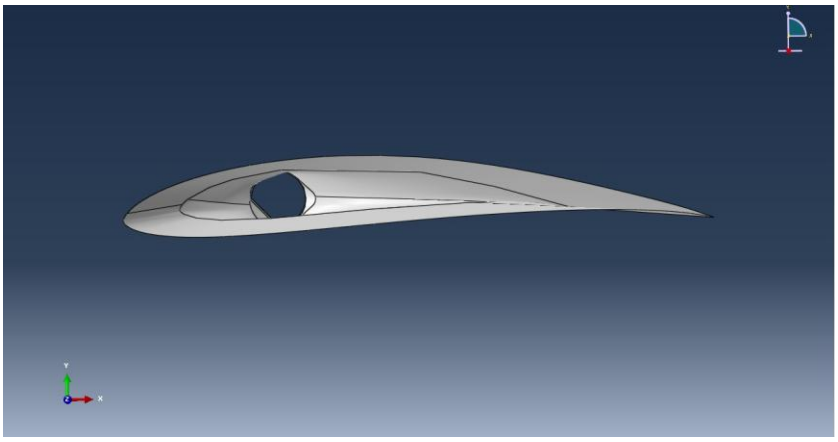

Figure 4.1 - Blade Created as a Hollow Shell with Open Ends to Replicate Physical Blade

A material was created in the material manager and was considered to be a three dimensional linear elastic material. The material was specified in each direction by the following properties: Young's modulus, Poisson's ratio, shear modulus, and strength. The exact values for each property can be found in the material data sheet provided by Cytec Engineering Materials for their Cycom 5320 Pre-peg epoxy resin system [19]. The composite layup was created using the defined material. To match blade design 1.0 and 1.1, a three ply, conventional shell composite layup was selected. The entire blade was selected for this layup. Each layer was selected to have the same material properties, each with a thickness of 1.27×10^{-3} inches. The first and third plies were selected to have a rotation angle of zero degrees, along the blade span. The second ply has a rotation angle of 90 degrees, perpendicular to the blade span. In the material properties two separate composite layups were created. To create blade design 1.2, two separate composite layups were created. The first layup consisted of the root and area leading up to the constant cross section. To match the blade design, a three ply, conventional shell composite layup was selected. Each layer was selected to have the same material properties, each with a thickness of 1.27×10^{-3} inches. The first and third plies were selected to have a rotation angle of zero degrees, along the blade span. The second ply had a rotation angle of 90 degrees, perpendicular to the blade span. The second composite layup consisted of the constant cross sectional area, the blade span. To match the blade design, a six ply, conventional shell composite layup was selected. Each layer was selected to have the same material properties, each with a thickness of 1.27×10^{-3} inches. The first, third, fourth, and sixth plies were selected to have a rotation angle of

zero degrees, along the blade span. The second and fifth ply has a rotation angle of 90 degrees, perpendicular to the blade span.

The loads and boundary conditions were then placed on the blade. A partition was created parallel to the blade ends at a location 9.5 inches from the blade root. This partition allowed for a reference location to place the loading. A static general step was created to replicate a static test. To replicate the static test on the blade 1.0, a displacement/rotation boundary condition was placed on the blade root. All displacements and rotations on this location were set to zero to replicate the blade clamping conditions as shown in Figure 4.2. For the blade design 1.1 and 1.2, a displacement/rotation boundary condition was placed on the blade root and the area leading up to the constant area cross-section. All displacements and rotations in this area were set to zero to replicate the blade clamping conditions as shown in Figure 4.3. Then a displacement/rotation was placed on the previously created datum plane. A displacement in the *y*-direction was created along the plane to replicate the loading conditions of the physical testing, discussed in the following section.

Next, the model was prepared to accept a mesh. A dependent mesh instance was created which allows the mesh to contour the model. This was created using seed edges. A finer mesh instance was placed on the blade root and locations surrounding the blade root. At these locations, an approximate element size of 0.01 was used. The remaining parts of the blade used an approximate element size of 0.07. A mesh instance tool was used to create the mesh, connecting all the seed edges, creating the blade mesh with 47759 elements, as shown in Figure 4.4. The model was then data checked to ensure it was free of errors that could cause invalid results. To archive the results, the field output

requests selected the Tsai-Hill failure modes, as well as blade force and strain at every element.

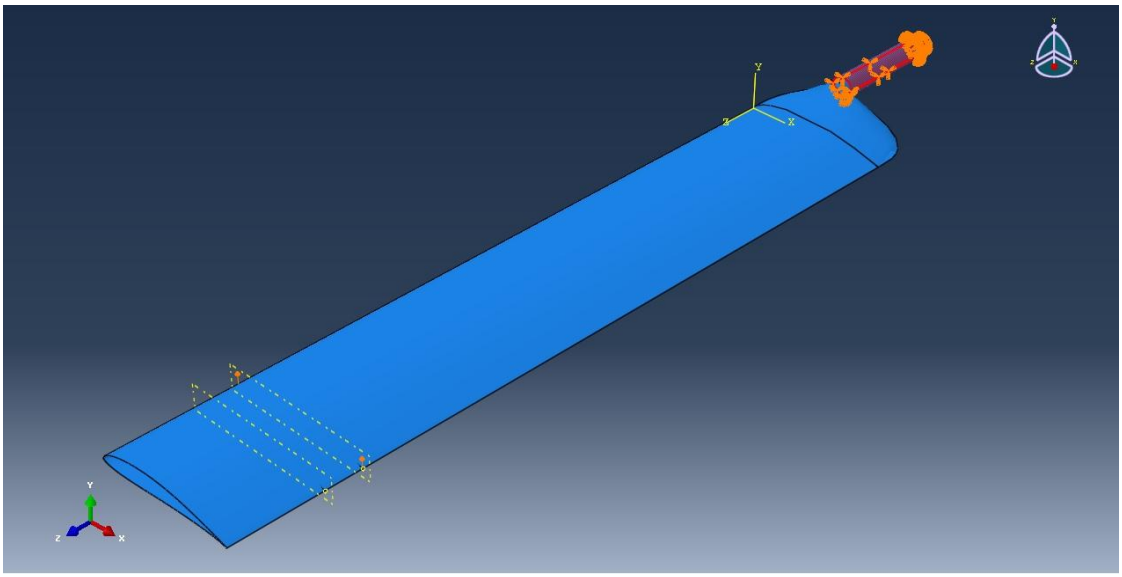

Figure 4.2 - Boundary Condition Located on Root for Blade Design 1.0

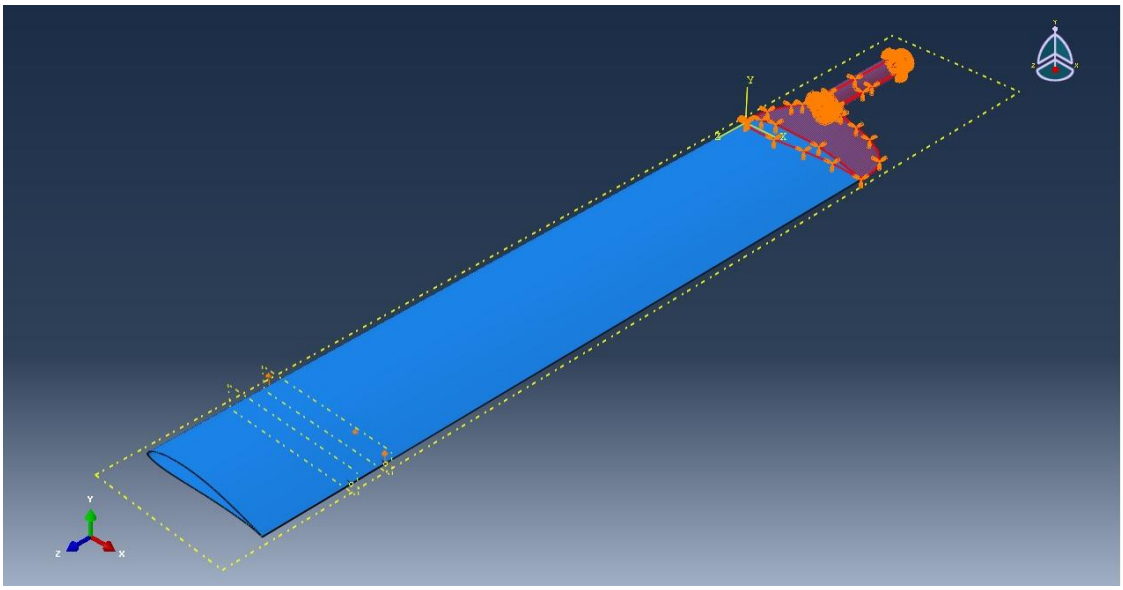

Figure 4.3 - Boundary Condition Located on Root and Area Leading to Constant Area Cross Section for Blade Design 1.1 and 1.2

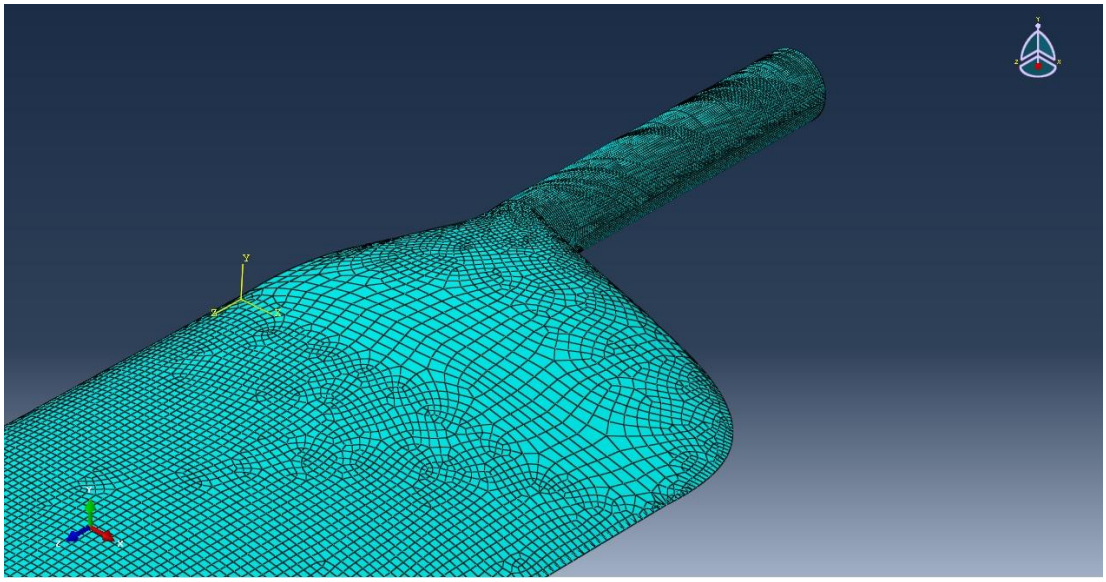

Figure 4.4 - Mesh Applied to Blade in ABAQUS

4.2. ANALYSIS PROCEDURE

To begin the analysis, a vertical displacement was applied at the loading location specified in the previous section. The vertical displacement was entered as the same displacement value as the physical tests. Here the force and strain at all locations on the blade can be found in the field outputs. To find the failure location, the displacement at the loading location was increased until the bladed failed according to the Tsai-Hill criterion. The Tsai-Hill criterion states that failure has occurred when the in-plane stresses dissatisfy the following inequality:

$$\frac{\sigma_1^2}{s_L^2} - \frac{\sigma_1\sigma_2}{s_L^2} + \frac{\sigma_2^2}{s_T^2} + \frac{\tau_{12}^2}{s_{LT}} \leq \mathbf{1} \tag{4}$$

Thus, when the Tsai-Hill criterion surpasses unity, the composite fails. The Tsai-Hill criterion value is found by viewing the output history.

5. EXPERIMENTAL TESTING

The objective of performing the static test on the composite blade was to determine the ultimate bending strength, the strain at specific locations along the blade span, and the blade flexure. To simulate the bending moments at the root, single point loading was used. These factors could be then used to determine the validity of the FEA predictions. Fatigue tests were performed on the composite blades to determine the number of cyclic loadings the blade could endure before failure. To simulate the fatigue loading, single point constant stress ratio loading was used. The number of cycles to failure determined the life of the blade. Each fatigue test was performed in conjunction with a series of unloading stiffness tests. The unloading stiffness test determined the rate at which the stiffness of the blade decreased.

The purpose of the axial fatigue testing of the aluminum specimens was to investigate the degradation in fatigue life by placing a hole in the proximity of a fillet radius. It was also determined if a hole in close proximity, but not interfering, with the fillet has any negative impact on the fatigue life. Hole locations were placed at various distances from the fillet to analyze the effects on fatigue life.

5.1. EXPERIMENTAL SETUP FOR TESTING COMPOSITE BLADE IN BENDING

Each individual blade was tested on an MTS 810 Machine, Figure 5.1. The MTS 810 is a high precision device that can perform material and component tests for static strength, fracture, fatigue, temperature, etc. MTS 810 machine specifications and capabilities can be found at [20]. Blade design 1.0 was clamped at the root using the

machined fixture in Figure 5.2. Blade designs 1.1 and 1.2 and the attached tabs were clamped in the machined fixture as shown in Figure 5.3. This fixture was used in both static and fatigue testing. The fixture was then fastened on to the test stand shown in Figure 5.4. For static testing using blade design 1.0, the free end of the blade was attached to an eccentric fixture placed in the MTS hydraulic wedge grips as shown in Figure 5.5. The eccentric fixture was used in conjunction with this blade design to prevent twisting in the blade, allowing the force to be applied in line with the blade root. For static and fatigue testing using blade design 1.1 and 1.2, the free end of the blade was attached to a centric fixture placed in the MTS hydraulic wedge grips as shown in Figure 5.6. The centric fixture was used in conjunction with these blade designs to apply the loading in line with the center of the blade span to prevent the blade from twisting.

For the static tests, the FlexTest SE controller, Figure 5.7, connected to the MTS machine was set up to output a plot of the applied force versus relative hydraulic displacement. To find the strain applied due to loading, three strain gauges were attached to the blade at locations 3, 5.5, and 8 inches from the blade root, Figure 5.8. The strain gauges were then wired to a P3 strain indicator and recorder, Figure 5.9. The P3 strain indicator was set up to output the three strain values simultaneously to the display and record the value to a multimedia card every second for the duration of the test.

For the fatigue tests, the FlexTest SE controller, Figure 5.7, connected to the MTS machine was set up to output the cycle number, the applied force, and relative hydraulic displacement. The cycle number was used to determine the number of applied loadings the composite blade could withstand before blade failure. The applied force and relative displacement of the ramp was used to find the unloading stiffness.

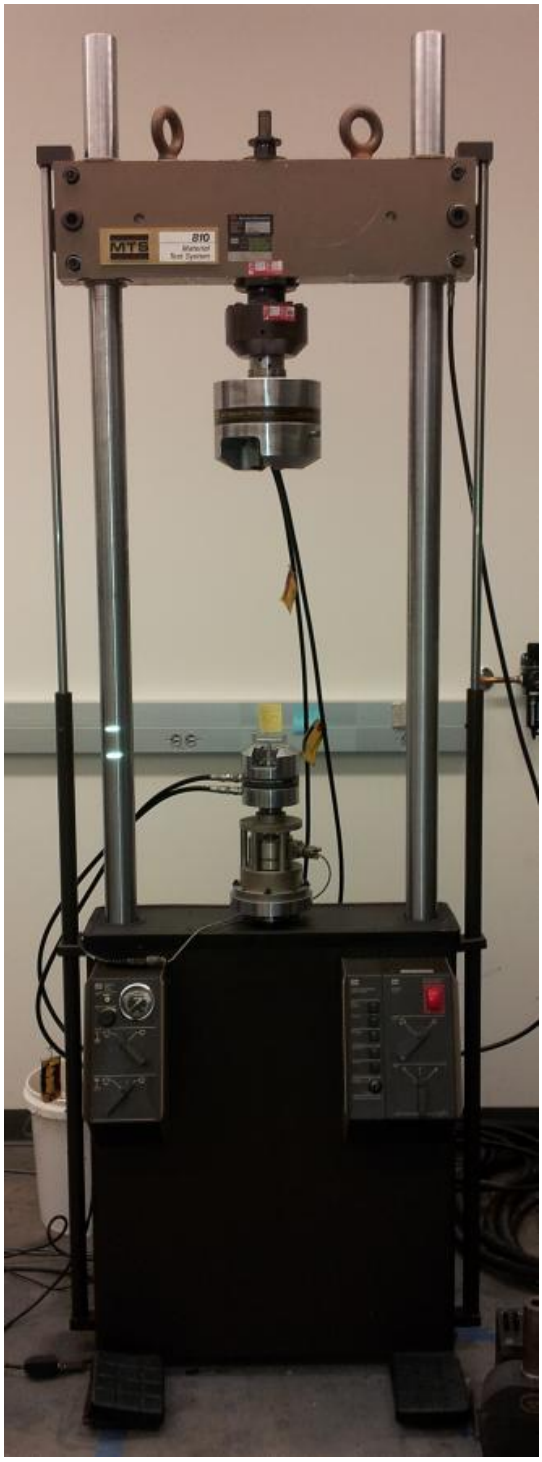

Figure 5.1 – MTS 810 Machine

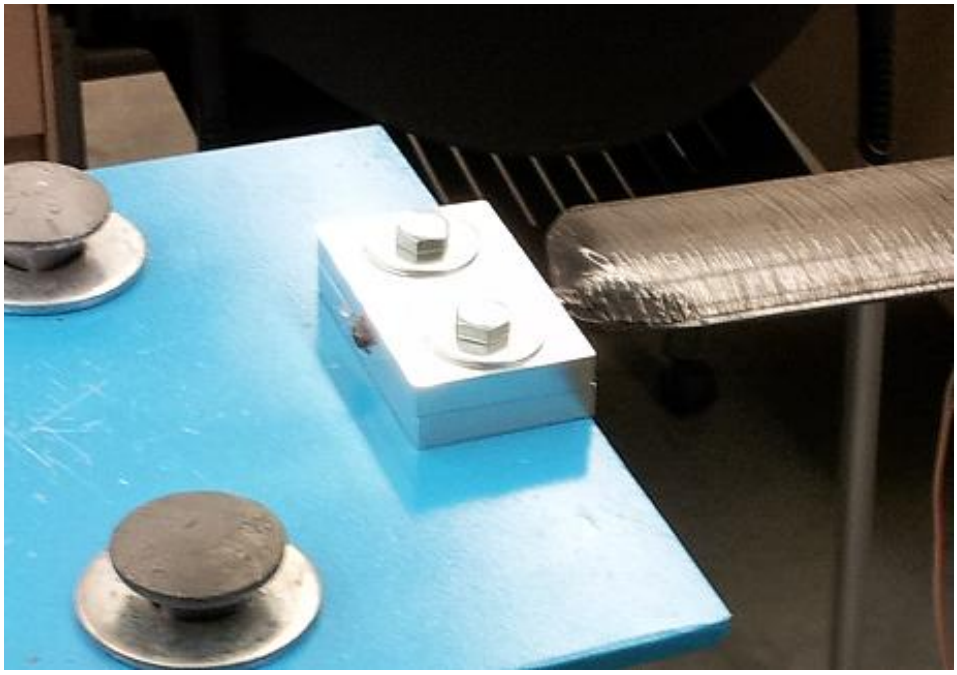

Figure 5.2 – Fixture used for Blade Design 1.0 that Secures the Blade at the Root

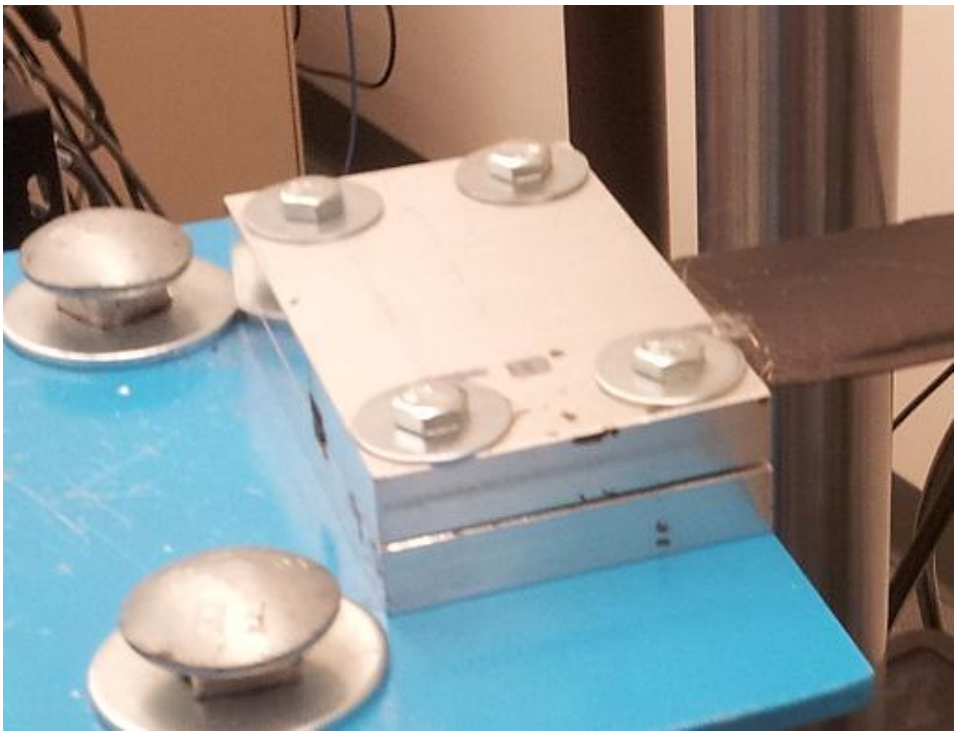

Figure 5.3 – Fixture used for Blade Design 1.1 and 1.2 that Isolates the Blade Span

Figure 5.4 – Test Stand used to Attach Blade Fixture and Allows for Single Point Bending to be Applied from MTS 810 Machine

Figure 5.5 – Eccentric Fixture used in Conjunction with Blade Design 1.0 to Prevent Blade Twisting

Figure 5.6 – Centric Fixture used in Conjunction with Blade Design 1.1 and 1.2 to Prevent Blade Twisting

Figure 5.7 – FlexTest SE Controller

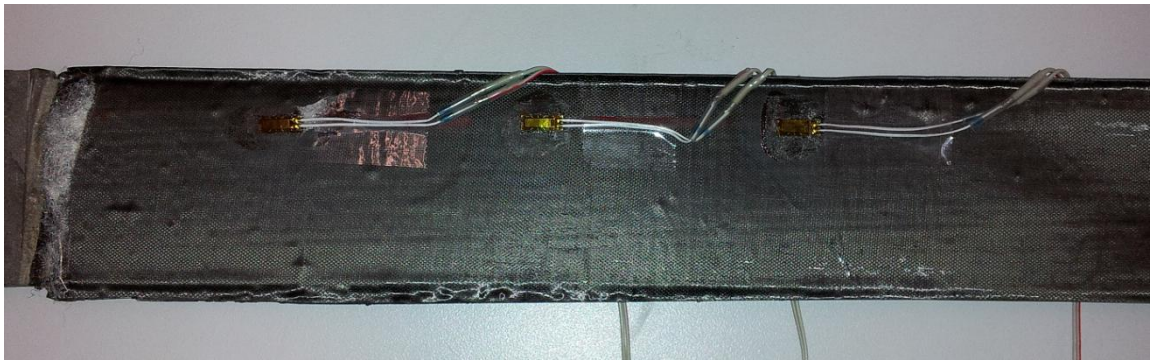

Figure 5.8 – Strain Gauges Applied to Composite Blade

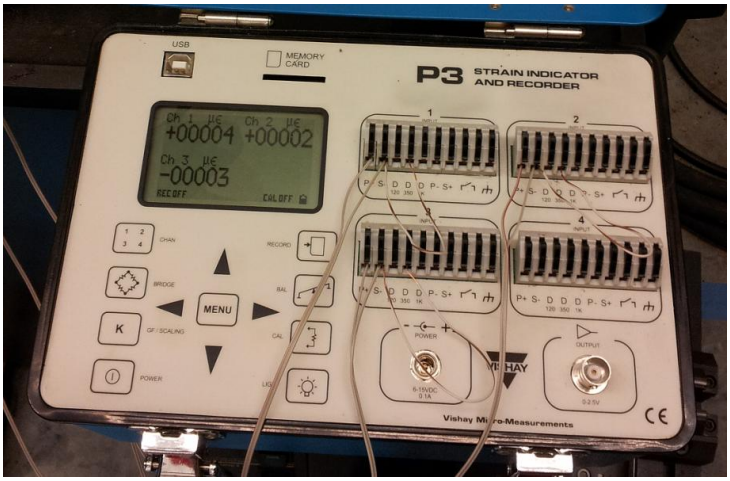

Figure 5.9 – P3 Strain Gauge Reader and Recorder

5.2. TEST PROCEDURE FOR COMPOSITE BLADE

For each test, static and fatigue, the blade was first secured onto the test stand. The MTS hydraulic power unit (HPU) control was turned on and reset to clear all channel interlocks. The MTS Flex Test SE was then set to the on position. The accompanying computer Station Manager application was started. Exclusive control was selected in the Station Manager and all interlocks were reset. The HPU and the HSM were set to high power. The hydraulic cylinder was set to the lowest point, for the full range of motion during the test.

For the static tests, the hydraulics were set to displace the blade at 10 mm/min. Next the strain gauges were connected to the strain gauge reader and were zeroed. The reader was set to take a reading once every second. These values were saved to a Multimedia Card for post processing. The Station manager was set to produce a real time plot of the force, in pounds, applied to the blade versus the vertical displacement, in inches, of the blade for post processing. The Station Manager was then set to run, and the test was initiated. The test concluded when the hydraulic cylinder reached a displacement of 6 inches, the MTS 810's maximum displacement.

For the Fatigue tests, four composite blades were fatigued at separate displacement levels. For each test, the Multipurpose Testware was set up to fatigue the specimens for a stress ratio of 0.1. A table of all fatigue test displacement levels and their corresponding maximum and minimum displacement is shown in Table 5.1. The first blade, fatigued at 65 percent of the failure displacement, was fatigued for one million cycles. Every ten thousand cycles, the cyclic displacement was stopped and an unloading stiffness test was performed. For the remainder of the fatigue tests, 80, 95 and 120

percent of the failure displacement, the blades were fatigued for two million cycles. For each test, the cyclic displacement was stopped every one hundred thousand cycles, and an unloading stiffness test was performed.

For all tests, the cyclic frequency was set to match the loading rate of the static test, 10 cycles per second. The machine was equipped with detectors to prevent the hydraulics from over-deflecting the blade and to stop the test once the test specimen had reached the set amount of cycles.

Table 5.1 - Displacement Levels and the Maximum and Minimum Displacements Applied in Fatigue Testing

Displacement Level	Maximum Displacement (in.)	Minimum Displacement (in.)
65%	0.340	0.018
80%	0.433	0.026
95%	0.544	0.034
120%	0.738	0.042

5.3. EXPERIMENTAL SETUP FOR AXIAL TESTING OF ALUMINUM SPECIMEN

Open hole specimens were machined using aluminum 2025-T231 plate material. Twenty four specimens were manufactured with hole to fillet dimensions including 0.5, 0.3079, 0.2029, 0.2091, and 0.1 inches. The test matrix can be seen in Table 5.2. Each specimen was engraved with the specimen ID to insure proper testing procedures. These specimens were fabricated to the specifications shown in Figure 3.7.

Each individual specimen was tested on an MTS 810 machine. The two ends of the specimens were secured using two hydraulic wedge grips at each end as shown in

Figure 5.10. The FlexTest SE controller, Figure 5.7, connected to the MTS machine was set up to output the cycle number, the applied force, and relative hydraulic displacement. The cycle number was used to determine the number of applied loadings the specimen could withstand before specimen failure. The applied force and relative hydraulic displacement were used to set detectors to determine when a crack nucleated in the specimen and when the specimen failed.

Table 5.2 - Open Hole Test Matrix [7]

Material	Specimen Drawing	X Dimension (in.)	Specimen ID	Quantity
2024-T351 Plate	Open Hole in Radius Test Specimen - 1	-	DW-RKt-1 to 6	5
	Open Hole in Radius Test Specimen - 2	.5000	DW-OH-5000-1 to 3	3
	Open Hole in Radius Test Specimen - 3	.3079	DW-OH-3079-1 to 3	4
	Open Hole in Radius Test Specimen - 4	.3029	DW-OH-3029-1 to 4	4
	Open Hole in Radius Test Specimen - 5	.2091	DW-OH-2091-1 to 4	4
	Open Hole in Radius Test Specimen - 6	.1000	DW-OH-1000-1 to 4	4
			Total	24

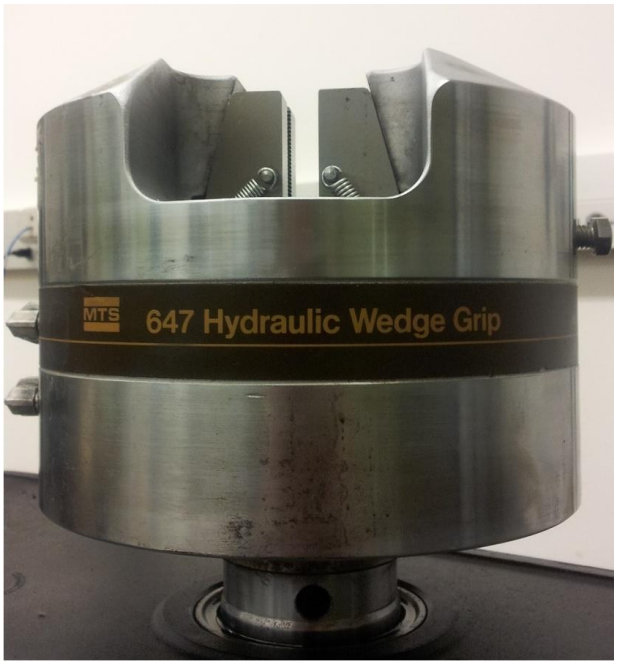

Figure 5.10 - Hydraulic Wedge Grips used on MTS 810 Machine

5.4. TEST PROCEDURE FOR ALUMINUM SPECIMENS

For testing, the MTS hydraulic power unit (HPU) control was turned on and reset to clear all channel interlocks. The MTS Flex Test SE was then set to the on position. The accompanying computer Station Manager application was started. Exclusive control was selected in the Station Manager and all interlocks were reset. The HPU and the HSM were set to high power. The hydraulic cylinder was set to the mid-point, for the equal range of motion during the test. One end of the specimen was placed and clamped in the hydraulic wedge grip. The hydraulic lift was then lowered to the specimen, and the other end of the specimen was secured.

A complete overview of the applied stress levels for the fatigue tests is shown in Table 5.3. Twenty four metallic specimens were fatigued at varying stress levels. For each test, the Multipurpose Testware was set up to fatigue the specimens for the stress ratio of 0.6 using load control. Each specimen was fatigued at a frequency of 10 Hz.

The first specimen with no holes drilled, DW-RKt-1, was tested at a stress level of 25 ksi. This specimen experienced one million cycles without failure, thus experiencing infinite life. The second specimen, DW-RKt-2 was tested at a stress level of 30 ksi. This specimen failed at a high number of cycles. Because of this, the last three specimens, DW-RKt-3 through 5, were tested at a stress level of 35 ksi. The stress level was increased to 35 ksi to induce fatigue failure at a reasonable number of cycles.

The first specimen with a hole drilled, DW-OH-5000-1, was tested at a stress level of 28 ksi. This specimen failed at a very low number of cycles. Because of this, the second specimen, DW-OH-5000-2, was tested at a stress level of 26 ksi. This specimen

still failed at a low number of cycles, so the final specimen, DW-OH-5000-3, was tested at a stress level of 25 ksi.

All of the remaining specimens with a hole drilled, DW-OH-3079-1 through 4, DW-OH-3029-1 through 4, DW-OH-2079-1 through 4, and DW-OH-1000-2 through 4, were tested at a stress level of 25 ksi. There was one exception with specimen DW-OH-1000-1. This specimen was tested at a stress level of 16 ksi. This specimen failed at a very high number of cycles, thus the increase in stress level to 25 ksi for the remaining specimens DW-OH-1000-2 through 4.

Table 5.3 - Fatigue Test Stresses Applied to Open Hole Specimens [7]

	Loading		Qty.
Specimen ID	S_{max} (ksi)	R	
DW-RKt-1	25	0.06	1
DW-RKt-2	30	0.06	1
DW-RKt-3 thru 5	35	0.06	3
DW-OH-5000-1	28	0.06	1
DW-OH-5000-2	26	0.06	1
DW-OH-5000-3	25	0.06	1
DW-OH-3079-1 thru 4	25	0.06	4
DW-OH-3029-1 thru 4	25	0.06	4
DW-OH-2091-1 thru 4	25	0.06	4
DW-OH-1000-1	16	0.06	1
DW-OH-1000-2 thru 4	25	0.06	3
		Total	24

6. ANALYSIS OF RESULTS

6.1. FINITE ELEMENT ANALYSIS OF THE COMPOSITE BLADE

The static failure loading case for each blade design was modeled in ABAQUS. Each blade was displaced to the deflection at which blade failure occurred in physical testing. The result for all three blade designs is shown in Table 6.1. Figures 6.1, 6.2, and 6.3 show the location, according to Tsai-Hill criterion, of failure on the blade structure for blade design 1.0, 1.1, and 1.2, respectively.

Table 6.1 - Force, Deflection and Strain Values Found at Failure for each Blade Design in FEA

Specimen	Deflection (in.)	Force (lb_f)	Strain 1 (με)	Strain 2 (με)	Strain 3 (με)
Blade Design 1.0	1.136	3.337	766	334	52
Blade Design 1.1	0.277	8.289	1029	777	312
Blade Design 1.2	0.600	21.986	1406	1203	83

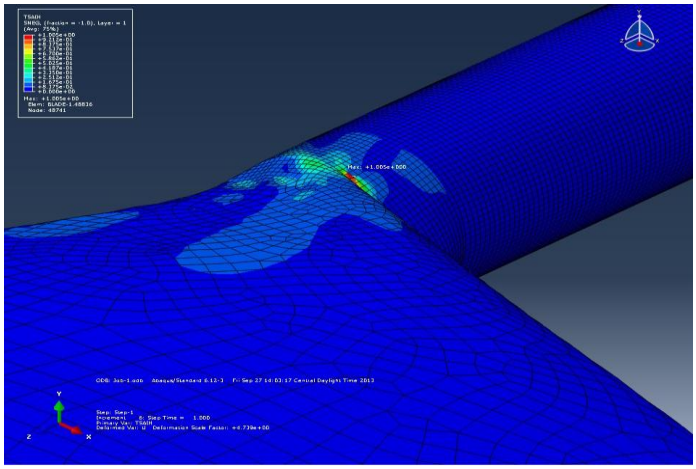

Figure 6.1 – Location of Failure for Blade Design 1.0 based on Tsai-Hill Failure Criterion

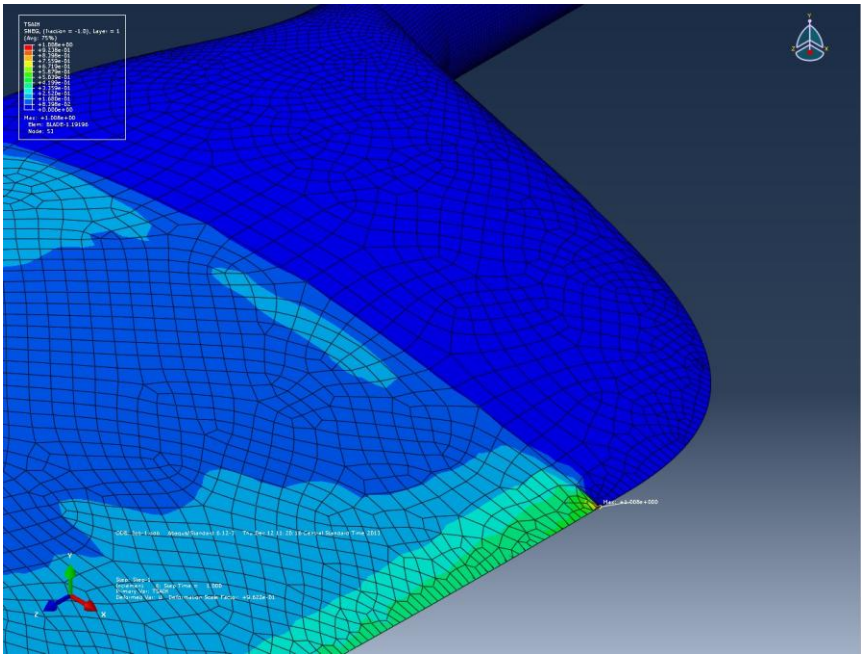

Figure 6.2 – Location of Failure for Blade Design 1.1 based on Tsai-Hill Failure Criterion

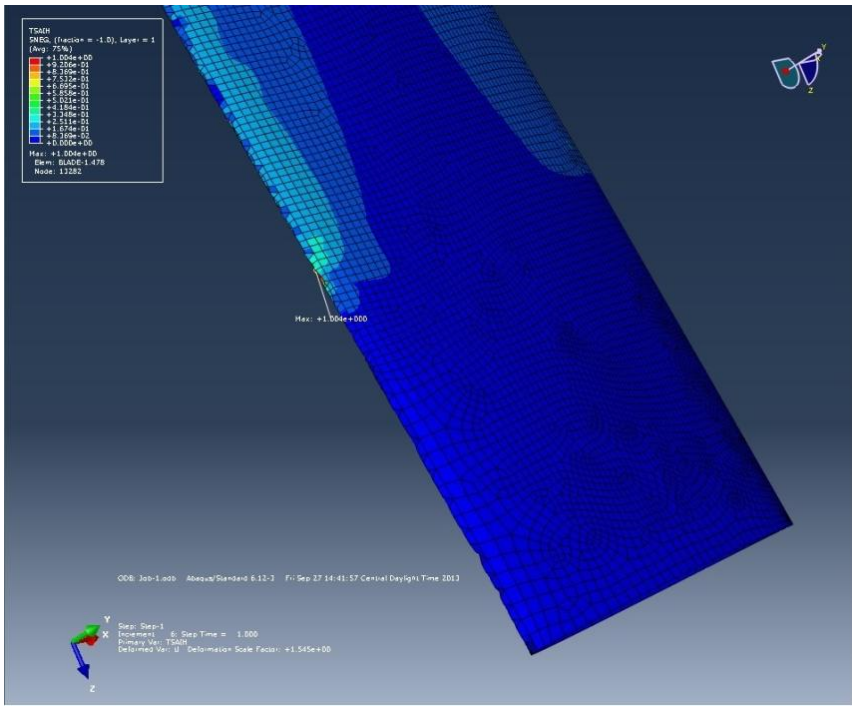

Figure 6.3 – Location of Failure for Blade Design 1.2 based on Tsai-Hill Failure Criterion

6.2. ANALYSIS OF STATIC TEST RESULTS FOR THE COMPOSITE BLADE

Three different blade designs were tested in the static loading case. The results of these tests are shown in Table 6.2. Figures 6.4 through Figures 6.7 show the graphical results of the tests up to blade failure. Figure 6.4 shows the force applied to the blade versus the upward deflection of the blade. Figures 6.5 through 6.7 show the strain versus the upward deflection of the blade for blade designs 1.0, 1.1, and 1.2, respectively.

Blade design 1.0 withstood a maximum force of 2.047 pounds at a blade deflection of 1.136 inches applied on the blade 9.5 inches from the blade root. The forces which caused blade failure were fairly similar between the FEA model and the static test, with the static test producing a load 38% lower than the FEA model. The difference comes into the recorded strain at a given blade displacement. It should also be noted that the strain gauge located 8 inches from the root was not producing accurate results. This is known because the strain gauge was giving a negative, compressive, value when the gauge was actually experiencing tensile forces. Because the strain gauge was reading incorrectly, the values were shifted by a constant amount, making all strain values positive. At this point, it was found that the strain values were all incorrect by a factor of five. By applying this correction factor, it can be shown that the strain values exhibit the same trend as the FEM, as shown in Table 6.3. Using this method, the strain error was found to be 0.5%, 15% and 100%, respectively. It should be noted that the FEA and static testing failed at the same location along the blade root.

Blade design 1.1 withstood a maximum force of 6.825 pounds at a blade deflection of 0.2769 inches, and blade design 1.2 withstood a maximum force of 20.199 pounds at a blade deflection of 0.6 inches. In both cases, the force was applied 9.5 inches

from the blade root. The forces at which blade design 1.1 and blade design 1.2 failed were very accurate in comparison between the FEA model and the static test. The failure force for blade design 1.1 and blade design 1.2 were 17% and 8% lower for the static test in comparison to the FEA model, respectively. The strain values between the FEA model and the static test differed greatly. It was found that all values between the two tests for both blades differed by a factor of two. By applying this correction factor, it can be shown that the strain values exhibit the same trend as the FEM, as shown in Table 6.3, producing a maximum error of 20% between all strain values. This suggests that there was an unforeseen error in calibration of the strain gauges.

It should be noted that the FEA model and static test failed at the same location along the blade root for blade design 1.1. For blade design 1.2, the physical test failed along the span at the blade root. The FEA model stated that the blade would fail along the leading edge of the blade, showing an incorrect failure location.

Table 6.2 - Force, Deflection and Strain values Recorded at Failure for each Blade Design in Static Testing

Specimen	**Deflection (in.)**	**Force (lb_f)**	**Strain 1 (με)**	**Strain 2 (με)**	**Strain 3 (με)**
Blade Design 1.0	1.136	2.047	179	85	25
Blade Design 1.1	0.277	6.825	426	316	131
Blade Design 1.2	0.600	20.199	572	564	34

Table 6.3 - Force, Deflection and Adjusted Strain values Recorded at Failure for each Blade Design in Static Testing

Specimen	Deflection (in.)	Force (lb_f)	Strain 1 (με)	Strain 2 (με)	Strain 3 (με)
Blade Design 1.0	1.136	2.047	775.000	390.000	5.000
Blade Design 1.1	0.277	6.825	958.5	711	294.75
Blade Design 1.2	0.600	20.199	1284.75	1266.75	74.25

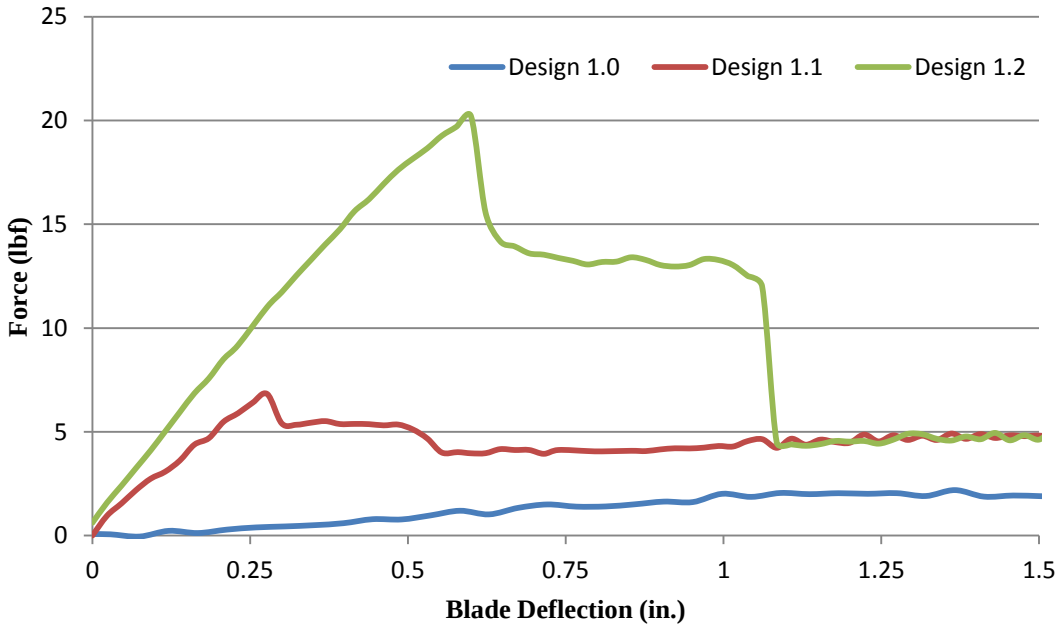

Figure 6.4 - Force vs. Blade Deflection to First Ply Failure Plot for all Blade Designs

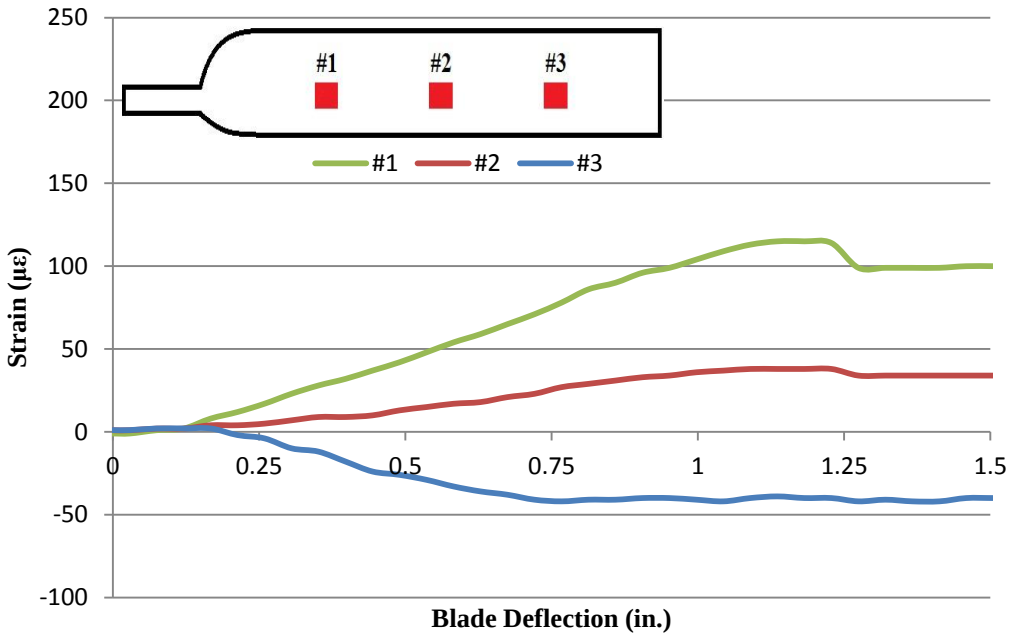

Figure 6.5 - Strain vs. Blade Deflection to First Ply Failure Plot for Blade Design 1.0

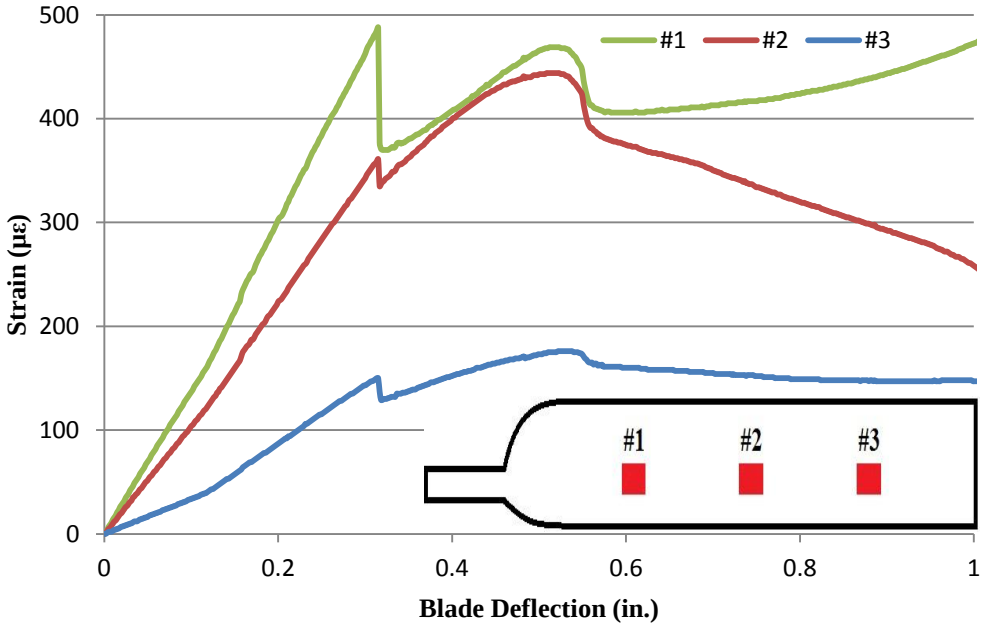

Figure 6.6 - Strain vs. Blade Deflection to First Ply Failure Plot for Blade Design 1.1

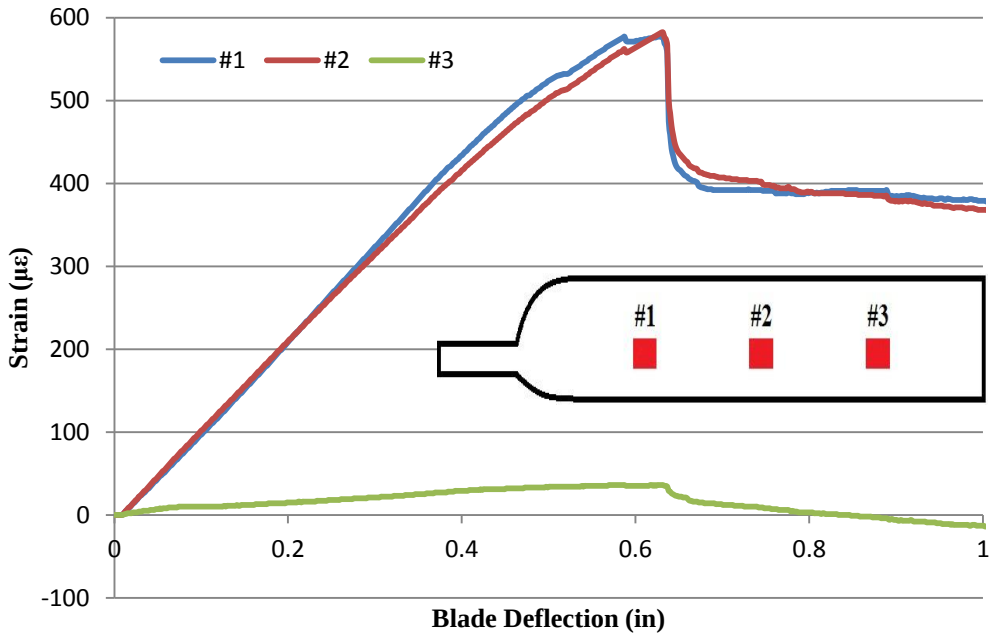

Figure 6.7 - Strain vs. Blade Deflection to First Ply Failure Plot for Blade Design 1.2

6.3. ANALYSIS OF FATIGUE TEST RESULTS FOR THE COMPOSITE BLADE

Four fatigue tests, with accompanying unloading stiffness tests, were performed at four different stress levels, 65, 80, 95, and 120 percent of the failure displacement. The first and second fatigue tests were performed at 65 and 80 percent of the failure force, respectively. At 65 percent, the blade survived one million cycles. At 80 percent, the number of test cycles was increased, and the blade survived two million cycles. One million cycles considers that the blade has an infinite life cycle. This means that the local stresses are essentially elastic and safely below the pertinent fatigue limit [21]. As shown in Figure 6.8, the unloading stiffness stayed relatively constant for both stress levels. This means that the blade experienced the same applied loadings for the given displacement range before and after one million cycles were applied. The third and final tests were

performed at 95 and 120 percent of the failure force, respectively. Both tests survived two million cycles without blade failure, thus both the blades have an infinite life cycle. Both tests showed a decrease in unloading stiffness over two million cycles. The blade fatigued at 120 percent of the failure stress decreased at a higher rate compared to the blade fatigued at 95 percent, for an equal number of cycles.

Because the blades did not fail due to fatigue, a static test to failure was performed for each blade following the fatigue tests. The purpose of the static test was to find if applying cyclic loading to the blades would decrease the stiffness and the force to failure. The numerical and graphical results of the static tests are shown in Table 6.4 and Figure 6.9, respectively. These static tests showed that the force to failure decreased after each fatigue test. Thus, the applied cyclic loadings decreased the overall strength of the blades. Along with the decreased failure force, the blade deflection at failure increased after each fatigue test. Thus, the applied fatigue decreased the overall stiffness of the blades.

Table 6.4 - Force and Displacement Values Recorded at Failure for Static Tests Conducted after Fatigue Tests

Load Level	**Force (lbf)**	**Deflection (in.)**
65%	12.639	0.6927
80%	13.958	0.7157
95%	17.088	0.6459
120%	14.894	0.7612

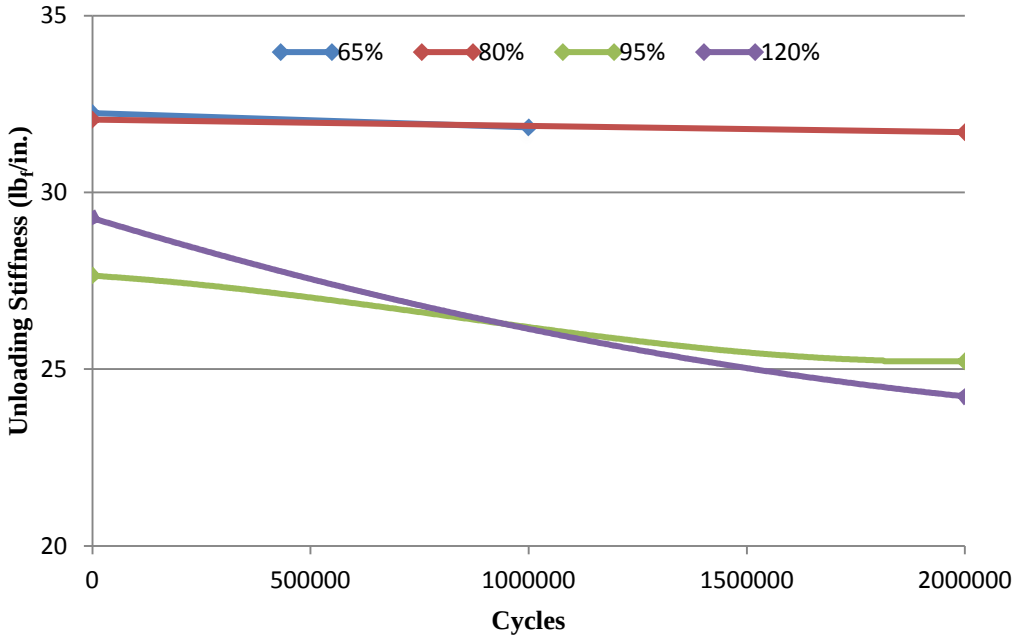

Figure 6.8 - Unloading Stiffness Plot for Each Cyclic Displacement Level Applied to Composite Blade

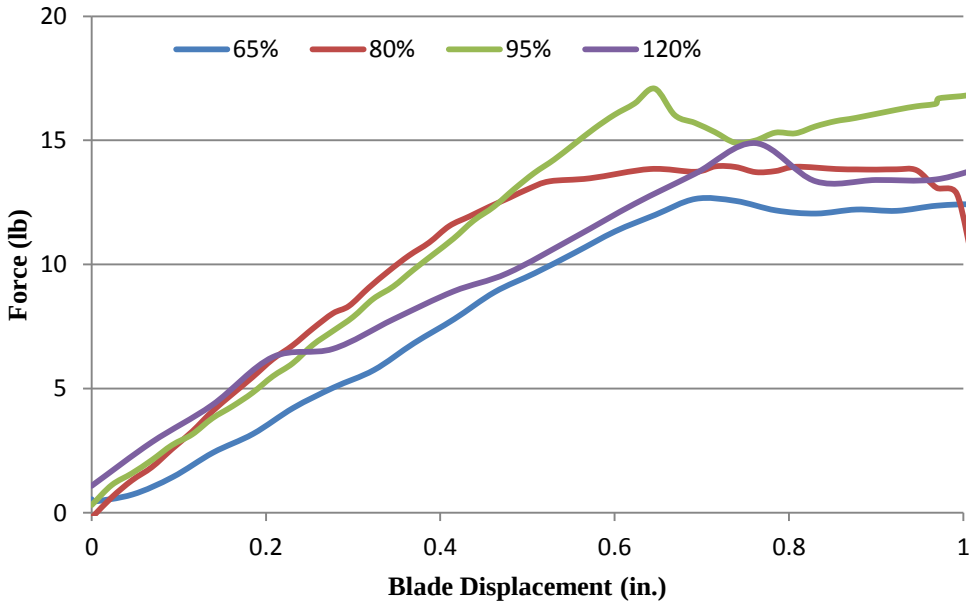

Figure 6.9 - Force vs. Blade Deflection to First Ply Failure Plot after Applied Fatigue for Each Cyclic Displacement Level

6.4. ANALYSIS OF FATIGUE TEST RESULTS FOR THE ALUMINUM SPECIMENS

Raw results for all fatigue tests of aluminum alloy specimens are presented in Table 6.5. This figure presents the test loads, *R*-ratios, number of cycles to crack initiation and number of cycles to specimen failure.

The first specimen with no holes drilled, DW-RKt-1, was tested at a stress level of 25 ksi. This specimen experienced 1,000,000 cycles without failure, thus experiencing infinite life. The second specimen, DW-RKt-2 was tested at a stress level of 30 ksi. This specimen failed at 523,201 cycles, still a relatively high number of cycles. Because of this, the last three specimens, DW-RKt-3 through 5, were tested at a stress level of 35 ksi. The stress level was increased to 35 ksi to induce fatigue failure at a reasonable number of cycles.

The first specimen with a hole drilled, DW-OH-5000-1, was tested at a stress level of 28 ksi. This specimen failed at 66,738 cycles, a very low number of cycles. Because of this, the second specimen, DW-OH-5000-2, was tested at a stress level of 26 ksi. This specimen still failed at 90,803 cycles, still a low number of cycles, so the final specimen, DW-OH-5000-3, was tested at a stress level of 25 ksi. This specimen failed at 114,987 cycles.

All of the remain specimens with a hole drilled, DW-OH-3079-1 through 4, DW-OH-3029-1 through 4, DW-OH-2079-1 through 4, and DW-OH-1000-2 through 4, were tested at a stress level of 25 ksi. There was one exception with specimen DW-OH-1000-1. This specimen was tested at a stress level of 16 ksi. This specimen failed at a high number of cycles, thus the stress level was increased to 25 ksi for the remaining specimens DW-OH-1000-2 through 4.

Table 6.5 - Open Hole Specimen Fatigue Test Results [7]

SPECIMEN NO.	Thickness	Width	C/S AREA (sq in)	MAX ksi	RATIO R	Pmax lbs	Pmin lbs	TEST START	TEST COMPLETE	CYCLES 1st CRACK	CYCLES FAILURE	Failure Location
DW-RKt-1	0.100	1.000	0.100	25.0	0.06	2,500	150	11/30/2012	12/1/2012	-	1,000,000	No Failure
DW-RKt-2	0.100	1.000	0.100	30.0	0.06	3,000	180	12/2/2012	12/2/2012	522747	523201	Lower Tangent of Radius
DW-RKt-3	0.100	1.000	0.100	35.0	0.06	3,500	210	12/3/2012	12/3/2012	364908	366702	Lower Tangent of Radius
DW-RKt-4	0.100	1.000	0.100	35.0	0.06	3,500	210	12/20/2012	12/21/2012	301115	301115	Lower Tangent of Radius
DW-RKt-5	0.100	1.000	0.100	35.0	0.06	3,500	210	12/21/2012	12/21/2012	317774	317804	Lower Tangent of Radius
DW-OH-5000-1	0.100	1.000	0.100	28.0	0.06	2,800	168	12/21/2012	12/21/2012	66638	66738	Edge of Hole
DW-OH-5000-2	0.100	1.000	0.100	26.0	0.06	2,600	156	12/21/2012	12/21/2012	79946	90803	Edge of Hole
DW-OH-5000-3	0.100	1.000	0.100	25.0	0.06	2,500	150	12/22/2012	12/22/2012	108510	114987	Edge of Hole
DW-OH-3079-1	0.100	1.000	0.100	25.0	0.06	2,500	150	12/22/2012	12/22/2012	103745	110211	Edge of Hole
DW-OH-3079-2	0.100	1.000	0.100	25.0	0.06	2,500	150	12/22/2012	12/22/2012	108905	114743	Edge of Hole
DW-OH-3079-3	0.100	1.000	0.100	25.0	0.06	2,500	150	12/22/2012	12/22/2012	107843	113461	Edge of Hole
DW-OH-3079-4	0.100	1.000	0.100	25.0	0.06	2,500	150	12/23/2012	12/23/2012	96035	103500	Edge of Hole
DW-OH-3029-1	0.100	1.000	0.100	25.0	0.06	2,500	150	12/23/2012	12/23/2012	107515	112060	Edge of Hole
DW-OH-3029-2	0.100	1.000	0.100	25.0	0.06	2,500	150	12/23/2012	12/23/2012	104640	108918	Edge of Hole
DW-OH-3029-3	0.100	1.000	0.100	25.0	0.06	2,500	150	12/23/2012	12/23/2012	94842	96291	Edge of Hole
DW-OH-3029-4	0.100	1.000	0.100	25.0	0.06	2,500	150	12/24/2012	12/24/2012	129522	133860	Edge of Hole
DW-OH-2091-1	0.100	1.000	0.100	25.0	0.06	2,500	150	12/27/2012	12/27/2012	104290	112904	Edge of Hole
DW-OH-2091-2	0.100	1.000	0.100	25.0	0.06	2,500	150	12/27/2012	12/27/2012	100094	100232	Edge of Hole
DW-OH-2091-3	0.100	1.000	0.100	25.0	0.06	2,500	150	12/27/2012	12/27/2012	92835	93418	Edge of Hole
DW-OH-2091-4	0.100	1.000	0.100	25.0	0.06	2,500	150	12/27/2012	12/28/2012	105230	105557	Edge of Hole
DW-OH-1000-1	0.157	1.000	0.157	16.0	0.06	2,500	150	12/28/2012	12/28/2012	225927	240193	Edge of Hole
DW-OH-1000-2	0.157	1.000	0.157	25.0	0.06	3,913	235	12/28/2012	12/28/2012	54333	54721	Edge of Hole
DW-OH-1000-3	0.157	1.000	0.157	25.0	0.06	3,913	235	12/28/2012	12/28/2012	58903	60974	Edge of Hole
DW-OH-1000-4	0.157	1.000	0.157	25.0	0.06	3,913	235	12/28/2012	12/28/2012	56301	59822	Edge of Hole

Using the preceding data, the characteristic lives for all five specimen groups were calculated using the Weibayes analysis method [22]. The characteristic life was used in conjunction with the equivalent stress fatigue life method [23] to calculate the following K_t mod factors, as shown in Table 6.6. A more in-depth analysis for determining the stress concentration modification factors is shown in [7].

Table 6.6 - Open Hole Specimen Stress Concentration Modification Factors [7]

Specimen Group	Characteristic Life	K_{tf}
DW-RKt-1 thru 5	310469	NA
DW-OH-5000-1 thru 3	117897	NA
DW-OH-3079-1 thru 4	110731	1.01
DW-OH-3029-1 thru 4	115240	1.00
DW-OH-2091-1 thru 4	103765	1.02
DW-OH-1000-1 thru 4	54693	1.15

7. CONCLUDING REMARKS

First, the conclusions for the composite blade are presented. The results between that FE model and the static tests were very accurate. In all the blade designs, both the FEA and static test failed at very similar forces. All tests were within 38 percent of each other. All the strains found in the static tests were very inaccurate compared to the FEA model. It was found that the stain results show the same trends when a correction factor was applied, suggesting that the strain gauges were improperly calibrated. Because the forces between the static test and FEA model were accurate and the strains exhibit similar trends, it can be concluded that the FEA accurately models the static tests up to first ply failure when using this configuration.

Each iteration of the blade design yielded significantly better performance, addressing major flaws of the preceding design. The second iteration isolated the blade root, eliminated a major stress concentration, and more than doubled the force the blade could withstand. The third iteration prevented the blade from splitting along the seams, eliminating epoxy failure. This caused the blade to fail along the blade span, allowed the blade material to carry the forces, and more than doubled the failure strength of the blade.

Fatigue testing showed that these composite blades do not fatigue unless tested near the failure force. The two tests at 65 and 80 percent of the failure force showed no signs of fatigue, even after two million cycles. Near and above the failure force, the blades did show some signs of fatigue. At 95 percent of the failure force, the blade stiffness decreased at a constant rate, decreasing by 8 percent over two million cycles. At 120 percent of the failure force, the blade unloading stiffness decreased drastically after the first cycle due to first ply blade failure. From 100,000 cycles to two million cycles the

unloading compliance decreased by 18 percent. Static tests performed after the fatigue tests showed that the blade's failure force did decrease due to the fatigue tests. On average, the blade failure strength decreased by 28 percent after 2 million cycles.

Finally, the conclusions for the axial fatigue testing are presented. Based on the stress concentration modification factors calculated from the physical tests, it was observed that specimens DW-OH-3079-1 through 4 and DW-OH-3029-1 through 4 showed virtually no interaction between the hole and the radius, with final K_{tf} values less than or equal to 1.01. For these two groups, the hole was placed near or just touching the fillet radius. For specimens DW-OH-2091-1 through 4, minor interactions were indicated with a final K_{tf} value of 1.02. For this group, the hole was centered on the fillet radius. For specimens DW-OH-1000-1 through 4, a definite interaction was indicated between the hole and the fillet radius, with a final K_{tf} value of 1.15. For this group, the hole was drilled directly through the slope of the fillet radius. Thus, for fatigue analysis of a hole interacting with a fillet, the most conservative K_{tf} of 1.15 is recommended.

BIBLIOGRAPHY

[1] G. Resch, A. Held, T. Faber, C. Panzer, F. Toro, and R. Haas, “Potentials and prospects for renewable energies at global scale,” Energy Policy, Vol. 36, p. 4048-4056, 2008.

[2] M. J. Khan, G. Bhuyan, M. T. Iqbal, and J. E. Quaicoe, “Hydrokinetic energy conversion systems and assessment of horizontal and vertical axis turbines for river and tidal applications: A technology status review,” Applied Energy, Vol. 86, p. 1823-1835, 2009.

[3] H. Li, G. A. Taylor, A M Abutunis, and K Chandrashekhara, “Design and Performance Evaluation of a Hydrokinetic Composite Turbine System,” SAMPE Conference, May 2013.

[4] S. Mieras, T. Ashuri, P. Scheijground, and G. V. Bussel, “Structural Design Analysis of a novel Tidal Turbine,” Renewable Energy, Vol. 57, P. 151-162, September 2013.

[5] C. Kong , T. Kim, D. Han, and Y. Sugiyama, “Investigation of fatigue life for a medium scale composite wind turbine blade,” International Journal of Fatigue, Vol. 28, p. 1382-1388, 2006.

[6] ESDU, "Guide to Stress Concentration Data," Engineering Sciences Data Item 64001, 1976.

[7] D. Whitley, "Interacting Stress Concentration Factors and their Effect on Fatigue of Metallic Aerostructures," Dissertation, Missouri University of Science and Technology, United States, 2013.

[8] W. D. Pilkey, "Peterson's Stress Concentration Factors," 2nd Edition, John Wiley & Sons, 1997.

[9] W. D. Pilkey, D. F. Pilkey "Peterson's Stress Concentration Factors," 3rd Edition, John Wiley & Sons, 2008.

[10] R. H. Graham, M. Raines, K. G. Swift, L. Gill, "Prediction of Stress Concentrations associated with Interacting Stress-Raisers within Aircraft Design: Methodology development and application," Proceedings of the Institution of Mechanical Engineers, Part G: Journal of Aerospace Engineering, 2005.

[11] R. H. Graham, “Interaction of Stress-Raising Features in Aerostructures” PhD Thesis, University of Hull, UK, 2002.

[12] C. Zhang, A Hajdaei, K. Zhang, and P. J. Hogg, "Fatigue Design of Wind Turbine Blades," Loughborough University, Powerpoint presentation, 2011.

[13] J. A. V. Alé, C. A. Santos, J. G. A. C. Filho, and G. C. S. Simioni, “Aerodynamic Loads and Fatigue of Small Wind Turbine Blades: Standard and Testing Procedures,” Europe's Premier Wind Energy Event (EWEA), Brussels, Belgium, March 2011.

[14] H. Mahfuz and M. Akram, “Life prediction of Composite Turbine Blades under Random Ocean Current and Velocity Shear,” Southeast National Marine Renewable Energy Center (SNMREC), Florida Atlantic University, Boca Raton, Florida, 2011.

[15] P. S. Veers, “A General Method for Fatigue Analysis of Vertical Axis Wind Turbine Blades,” Applied Mechanics Division IV 1524, Sandia National Laboratories, Albuquerque, New Mexico, 1983.

[16] C. R. Kennedy, S. B. Leen, C. M. Ó. Brádaig, “A Study of the Fatigue Life of Glass Reinforced Polymer Composites for Tidal Turbine Blades,” Proceedings of the ASME 30th International Conference on Ocean, Offshore, and Arctic Engineering, Rotterdam, The Netherlands, 2011.

[17] J. Paquette, J. van Dam, S. Hughes, and J. Johnson, “Fatigue Testing of 9 m Carbon Wind Turbine Research Blades,” 46th AIAA Aerospace Sciences Meeting and Exhibit, Reno, Nevada, 2008.

[18] R. I. Stephens, A. Fatemi, R. R. Stephens, and H. O. Fuchs, "Metal Fatigue in Engineering", 2nd Edition, Wiley-Interscience, New York, 2001.

[19] Cytec Industries, Cycom 5320-1, www.cytec.com, 2013.

[20] MTS Systems Corporation, www.mts.com, 2013.

[21] T. L. Anderson, Fracture Mechanics, 3rd Edition, Taylor & Francis, Boca Raton, 2005.

[22] R. B. Abernethy, “The New Weibull Handbook”, Fifth Edition, 2007.

[23] Federal Aviation Administration, "MMPDS-03," Battelle Memorial Institute, Columbus, OH, October, 2006.

VITA

Ross Henry Falen was born in Blue Springs, Missouri. He remained in Blue Springs throughout his elementary and secondary education. In 2008, Mr. Falen graduated with honors from Blue Springs South High School. He received a Bachelor of Science degree in Aerospace Engineering from Missouri University of Science and Technology in May 2012, graduating magna cum laude. Mr. Falen remained at Missouri S&T to pursue his graduate studies. He worked as a Graduate Teaching Assistant, teaching Mechanical Instrumentation laboratory for three semesters.

As a junior undergraduate, Mr. Falen was a member of the Missouri S&T Satellite Project (ARFL competition and design team). He held positions in both the structures and propulsion subsystem and remained involved with the team activities through his first year of graduate school.

Mr. Falen earned a Master of Science in Mechanical Engineering from the Missouri University of Science and Technology in May 2014. His thesis title was "Effect of Stress Concentrations on Fatigue of Composite and Metallic Structures," advised by Dr. Lokesh R. Dharani.